Circulation Research
JOURNAL OF THE AMERICAN HEART ASSOCIATION

Remodeling of the Mononuclear Phagocyte Network Underlies Chronic Inflammation and Disease Progression in Heart Failure: Critical Importance of the Cardiosplenic Axis

Mohamed Ameen Ismahil, Tariq Hamid, Shyam S. Bansal, Bindiya Patel, Justin R. Kingery and Sumanth D. Prabhu

Circ Res. 2014;114:266-282; originally published online November 1, 2013;
doi: 10.1161/CIRCRESAHA.113.301720
Circulation Research is published by the American Heart Association, 7272 Greenville Avenue, Dallas, TX 75231

Print ISSN: 0009-7330. Online ISSN: 1524-4571

Remodeling of the Mononuclear Phagocyte Network Underlies Chronic Inflammation and Disease Progression in Heart Failure

Critical Importance of the Cardiosplenic Axis

Mohamed Ameen Ismahil, Tariq Hamid, Shyam S. Bansal, Bindiya Patel, Justin R. Kingery, Sumanth D. Prabhu

Rationale: **The role of mononuclear phagocytes in chronic heart failure (HF) is unknown.**

Objective: **Our aim was to delineate monocyte, macrophage, and dendritic cell trafficking in HF and define the contribution of the spleen to cardiac remodeling.**

Methods and Results: **We evaluated C57Bl/6 mice with chronic HF 8 weeks after coronary ligation. As compared with sham-operated controls, HF mice exhibited: (1) increased proinflammatory CD11b$^+$F4/80$^+$CD206$^-$ macrophages and CD11b$^+$F4/80$^+$Gr-1^{hi} monocytes in the heart and peripheral blood, respectively, and reduced CD11b$^+$F4/80$^+$Gr-1^{hi} monocytes in the spleen; (2) significantly increased CD11c$^+$B220$^-$ classical dendritic cells and CD11c$^{+/low}$B220$^+$ plasmacytoid dendritic cells in both the heart and spleen, and increased classic dendritic cells and plasmacytoid dendritic cells in peripheral blood and bone marrow, respectively; (3) increased CD4$^+$ helper and CD8$^+$ cytotoxic T-cells in the spleen; and (4) profound splenic remodeling with abundant white pulp follicles, markedly increased size of the marginal zone and germinal centers, and increased expression of alarmins. Splenectomy in mice with established HF reversed pathological cardiac remodeling and inflammation. Splenocytes adoptively transferred from mice with HF, but not from sham-operated mice, homed to the heart and induced long-term left ventricular dilatation, dysfunction, and fibrosis in naive recipients. Recipient mice also exhibited monocyte activation and splenic remodeling similar to HF mice.**

Conclusions: **Activation of mononuclear phagocytes is central to the progression of cardiac remodeling in HF, and heightened antigen processing in the spleen plays a critical role in this process. Splenocytes (presumably splenic monocytes and dendritic cells) promote immune-mediated injurious responses in the failing heart and retain this memory on adoptive transfer. (*Circ Res*. 2014;114:266-282.)**

Key Words: dendritic cells ■ heart failure ■ inflammation ■ monocytes ■ spleen

Persistent inflammation is a hallmark of chronic heart failure (HF).[1] In humans, augmented levels of circulating and myocardial proinflammatory cytokines correlate with HF disease stage and mortality.[2] Moreover, animal studies support a causal role for inflammatory mediators in many of the pathological responses in the failing heart.[1,3] These observations formed the basis for the cytokine hypothesis of HF[4] and suggested therapeutic promise for cytokine antagonism. Paradoxically, however, clinical trials of antibody-based neutralization of tumor necrosis factor (TNF), a foundation proinflammatory cytokine, failed to show any therapeutic benefit (and was even harmful at high doses).[1,4] This unexpected clinical response alludes to an over-riding and underappreciated complexity of cytokine networks in HF[5] that cannot be effectively targeted in an all-or-none manner. To date, despite a wealth of studies establishing pathological inflammatory activation in HF, no large-scale immunomodulatory therapies have been successfully translated to clinical practice.

In This Issue, see p 227
Editorial, see p 230

The main translational focus of immune modulation in HF has thus far been directed toward protein mediators such as cytokines. In contrast, much less attention has been given to

Original received May 4, 2013; revision received October 30, 2013; accepted November 1, 2013. In October 2013, the average time from submission to first decision for all original research papers submitted to *Circulation Research* was 12.81 days.

From the Division of Cardiovascular Disease, Department of Medicine, University of Alabama at Birmingham and Birmingham VAMC, Birmingham, AL (M.A.I., T.H., S.S.S., B.P., S.D.P.); and Department of Medicine, University of Louisville, KY (J.R.K.).

This manuscript was sent to Ali J. Marian, Consulting Editor, for review by expert referees, editorial decision, and final disposition.

The online-only Data Supplement is available with this article at http://circres.ahajournals.org/lookup/suppl/doi:10.1161/CIRCRESAHA.113.301720/-/DC1.

Correspondence to Sumanth D. Prabhu, MD, Division of Cardiovascular Disease, University of Alabama at Birmingham, 311 Tinsley Harrison Tower, 1900 University Blvd, Birmingham, AL 35294-0006. E-mail sprabhu@uab.edu

Nonstandard Abbreviations and Acronyms	
BM	bone marrow
cDC	classical DC
DC	dendritic cell
HF	heart failure
HMGB1	high mobility group box-1
MCP-1	monocyte chemoattractant protein-1
pDC	plasmacytoid DC
SRP	subcapsular red pulp
TNF	tumor necrosis factor

modulating the underlying immune and inflammatory cell network that serves both as an important source and effector target for cytokines. As HF is a systemic disease triggered by cardiac dysfunction, chronic cytokine elaboration suggests global alterations in inflammatory cell populations both within and beyond the failing heart, such as in lymphoid tissue and bone marrow (BM). Prominent among these cell types are monocyte/macrophage and dendritic cell (DC) populations (mononuclear phagocytes) that are of signal importance in regulating (and generating) immune responses.[6–9] Macrophages and their direct precursor monocytes are central to tissue inflammation and innate immunity, whereas DCs are professional antigen-presenting and antigen-processing cells that are critical for adaptive immune responses and immune memory/tolerance. The functional roles of these cells are complex and heterogeneous, because different subtypes can either promote or suppress a variety of responses, including inflammation, cell clearance, wound healing, and autoimmunity.[6–9]

In acute myocardial infarction, both monocytes and DCs have been shown to contribute importantly to early postinfarction remodeling.[10–14] In contrast, whether and how the myelomonocytic network between lymphoid tissue, BM, and the heart is altered in chronic HF is unknown. Determining this is of utmost importance to understanding inflammatory dysregulation in HF and for targeting potential therapies directed at specific cell populations. Hence, we undertook a comprehensive analysis of the mononuclear phagocyte network in chronic HF and the contribution of the spleen, the largest secondary lymphoid organ in the body, to this network and to pathological left ventricular (LV) remodeling. Our results demonstrate, for the first time to our knowledge, profound alterations in cardiac and splenic mononuclear cells and splenic tissue niches in chronic HF that: (1) promote the circulation and residence of proinflammatory monocytes/macrophages, classical DCs (cDCs), and plasmacytoid DCs (pDCs); and (2) regulate both chronic inflammation and the progression of pathological LV remodeling.

Methods

All studies were performed in compliance with the National Institutes of Health (NIH) Guide for the Care and Use of Laboratory Animals (NIH Publication No. 85-23; revised 1996). The University of Alabama at Birmingham Institutional Animal Care and Use Committee gave local approval for these studies. A total of 120 mice were used.

Mouse Models and Surgical Protocol

Male C57BL/6J mice 10 to 12 weeks of age (Jackson Laboratories; stock #000664) were used. To induce pathological LV remodeling and HF, the mice underwent left thoracotomy and left coronary artery ligation (n=19) as previously described.[3,15,16] Sham-operated mice (n=12) were used as controls. The mice were followed for 8 weeks after operation and evaluated for various readouts.

Echocardiography

Mouse echocardiography was performed under anesthesia with tribromoethanol (0.25 mg/g IP), and isoflurane (≈1%) as needed, using a VisualSonics Vevo 770 High-Resolution System with a RMV707B scanhead. Mice were imaged on a heated, bench-mounted adjustable rail system (Vevo Imaging Station) that allowed steerable and hands-free manipulation of the ultrasound transducer.

Isolation of Splenocytes

Eight weeks after coronary ligation or sham operation, the spleen was removed aseptically and placed in a 35-mm tissue culture dish with ≈5 mL DMEM culture medium (Gibco; Invitrogen). Splenocytes were isolated according to the protocol of Lavelle et al[17] with slight modifications. Briefly, the spleen was finely minced using a scalpel. Repeated pipetting was used to disperse cells from minced fragments, and single cells were transferred to a fresh tube and kept on ice. For larger tissue pieces, the procedure was repeated several times in the dish with fresh DMEM. The final cell suspension was pipetted through a nylon cell strainer, 100 μm (BD Falcon), into a fresh tube and centrifuged at 150*g* for 5 minutes at 4°C. The supernatant was decanted, and the pellet resuspended in 0.4 mL of RBC lysis buffer (eBiosciences) for 5 minutes at room temperature. The addition of fresh DMEM neutralized the erythrocyte lysis. Pelleted splenocytes were then resuspended in fresh DMEM (0.5–1.0 mL).

Isolation of BM and Peripheral Blood Cells

After mice were euthanized, femurs and tibiae were dissected from the adherent soft tissue. The tip of each bone was removed with scissors, and the marrow was flushed with DMEM using a 27-gauge needle and aspirated. BM cells were filtered through a 100-μm nylon cell strainer (BD Falcon), sedimented at 150*g* for 5 minutes at 4°C, and resuspended in RBC lysis buffer. After complete erythrocyte lysis, BM cells were resuspended in fresh 1 to 2 mL DMEM.

Peripheral blood (≈500 μL) was collected in BD Microtainer tubes with EDTA. Erythrocytes were lysed with 2 mL RBC lysis buffer for 5 minutes on ice. Leukocytes were collected by centrifugation (380*g* for 10 minutes at 4°C) and resuspended in 400 uL ice-cold flow cytometry staining buffer (eBiosciences).

Isolation of Mononuclear Cells From the Heart

Single mononuclear cells were isolated from sham and failing hearts following the method of Austyn et al.[18] Mouse hearts were excised in toto and placed in heparinized saline. After removal of epicardial fatty tissue and the aorta, the heart was finely minced into ≈1 to 2 mm pieces and blood was removed by repeated washing in saline (with stepwise reductions in added heparin). The tissue was digested with collagenase (1 mg/mL; Worthington), trypsin (0.1%; Gibco, Invitrogen), and DNAse (10 μg/mL; 5 Prime) in 10 mL RPMI media (Gibco) for 45 minutes at 37°C with occasional shaking. Released cells were separated from solid tissue by filtering through a 100-μm nylon cell strainer (BD Falcon), washed with R10 media (RPMI-1640 supplemented with 10% heat-inactivated FCS, 2 mmol/L L-glutamine, 25 μmol/L 2-mercaptoethanol, 1% penicillin/streptomycin), and placed on ice. These steps were repeated 2 to 3 times to digest the remaining tissue. Any residual solid tissue was treated sequentially with EDTA (2 mmol/L) in digestion media for 10 minutes at 37°C, with collagenase (2 mg/mL) in R10 media for 20 minutes at 37°C, and released cells filtered through the strainer. All collected cells were pooled and pelleted at 150*g* for 5 minutes at 4°C. Single-cell suspensions were layered on Ficoll gradient solution and centrifuged at 2000*g* for 20 minutes. To reduce myocyte contamination in the mononuclear cell suspension, 75% of the total volume (excepting cell debris) was collected and washed in R10 media. The presence of nucleated cells was confirmed by DAPI staining during flow cytometry analysis. In a separate aliquot, cell viability (>80%) was confirmed using the trypan blue exclusion method.

Flow Cytometry

Isolated cell suspensions were incubated for 30 minutes at room temperature in a cocktail of fluorophore-labeled monoclonal antibodies as appropriate for the specific study against F4/80-Pacific Blue (BD Biosciences), CD8-FITC (BD Biosciences), CD45R/B220-APC (BD Biosciences), CD11b-605-NC (eBiosciences), Gr-1-APC (eBiosciences), CD11c-PE-Cy7 (BD Biosciences), CD86-PE-Cy5 (BD Biosciences), CD206-FITC (BD Biosciences), Siglec-H-efluor 660 (eBiosciences), CD45.1-FITC (Miltenyi Biotech), and CD45.2-PE (BD Biosciences). Lineage 1 antibody cocktail was used for DC identification (to exclude thymocytes [CD90.2-PE], natural killer cells [NK1.1-PE], CD49B-PE, and granulocytes [Gr-1-PE)], and Lin2 antibody cocktail was used for macrophage/monocyte subset identification (CD90.2-PE, NK1.1-PE, CD49B-PE, and CD45R/B220-PE for B-cells). In separate assessments of splenic T-cells, cell suspensions were incubated with CD3-FITC, CD4-650 NC, and CD8-605 NC (eBiosciences). Of note, the anti-Gr-1 antibody recognizes both lymphocyte antigens 6C and 6G.[19]

Activated macrophages/monocytes were identified as $CD11b^+F4/80^+$ cells.[20,21] Proinflammatory monocytes were identified as $Lin2^-CD11b^+F4/80^+Gr\text{-}1^{hi}$ and anti-inflammatory monocytes as $Lin2^-CD11b^+F4/80^+Gr\text{-}1^{low}$ cells.[9,20–22] Proinflammatory M1 and anti-inflammatory M2 macrophages in tissue were subclassified from $Lin2^-CD11b^+F4/80^+$ cells based on the absence or presence of CD206 (mannose receptor) expression.[8] DCs were identified as $Lin1^-CD11c^+$ cells.[6,9,22] cDCs were identified as $Lin1^-CD11c^+B220^-$, whereas nonclassical pDCs were identified as $Lin1^-CD11c^{+/low}B220^+$.[6,22–24] In some studies, pDCs were identified as Siglec-H^+ cells.[25] Lymphoid cDCs were further subdivided as $CD8^+$ or $CD8^-$,[6,22] and pDCs as $CD86^+$ or $CD86^-$ (classical costimulatory molecule and marker of pDC maturity).[26] Helper and cytotoxic T-cells were characterized as $CD3^+CD4^+$ and $CD3^+CD8^+CD4^-$ cells, respectively.[27] For the heart, spleen, and BM, identified cells were normalized for total cell population. For peripheral blood, cell numbers were normalized for the total lymphocyte and monocyte gate. Data were acquired on an LSRII flow cytometer (BD Biosciences) and analyzed with FlowJo software, version 7.6.3.

Immunohistochemistry and Confocal Microscopy

Formalin-fixed, paraffin-embedded hearts and spleens from sham and HF mice were sectioned at 5 μm thickness, deparaffinized, and rehydrated; (immuno)histological staining was performed as previously described.[3,15] Masson trichrome was used to evaluate tissue fibrosis and general histology (heart and spleen), and Alexa Fluor 488–conjugated wheat germ agglutinin (Invitrogen) for myocyte area. Myocardial apoptosis was evaluated using the DeadEnd Fluorometric TUNEL System (Promega) as previously described.[15,28] Sections were also blocked and then incubated with antibodies against CD11b/ITAM (Epitomics), CD11c (eBiosciences), F4/80 (eBiosciences), CD169 (R&D Systems), high mobility group box-1 (HMGB1; IBL International), and CD45.2-PE (BD Biosciences), and secondary antibodies were conjugated with Alexa 488, 555, or 647 (Invitrogen). Nuclei were stained with DAPI. Myocyte area and cardiac fibrosis were quantified from 5 to 6 high-power fields per section in the remote noninfarcted area of the heart using ImageJ and Metamorph software, respectively. In the spleen, CD11b-positive cells in the subcapsular red pulp (SRP) were counted in 3 to 5 high-power fields per section. Data for each group were calculated from 12 to 15 sections and 4 to 5 mice from each group. The measurements and calculations were conducted in a blinded manner. Confocal microscopy was performed on an LSM710 microscope (Zeiss), and Z-stack images were acquired according to standard protocols.

Cytometric Bead Array Immunoassay for Serum Cytokines

Peripheral blood was allowed to clot at room temperature for 2 hours. After centrifugation at 2000*g* for 10 minutes, serum was collected and stored at −20°C until assays were performed. Serum concentrations of TNF, monocyte chemoattractant protein (MCP)-1, interferon (IFN)-γ, interleukin (IL)-6, IL-10, and IL-12p70 were measured simultaneously using a Cytometric Bead Array Mouse Inflammation Kit (BD Biosciences). Briefly, 50 μL of chemokine capture bead mixture was incubated with 50 μL of either recombinant standard or sample and 50 μL of R-rhycoerythrin (PE)-conjugated detection antibody for 2 hours at room temperature. The mixture was washed to remove unbound PE detection reagent before data acquisition on a BD LSRII flow cytometer. Analysis was performed using FCAP Array software.

Splenocyte Gene Expression by Quantitative Real-Time PCR

Mononuclear splenocytes were cultured in serum-free DMEM media for 24 hours after isolation (2 to 3×10^6 cells/well). The cells were then collected and stored at −80°C in TRIzol reagent (Invitrogen) for subsequent RNA isolation. cDNA synthesis and quantitative real-time PCR were performed as previously described.[3,16,28] Relative levels of mRNA transcripts for TNF, IL-1β, IL-2, IL-4, IL-5, IL-6, IL-10, IL-13, IFN-γ, inducible nitric oxide synthase (iNOS), C-C chemokine receptor type 2, CCR5, chemokine (C-C motif) ligand 5, chemokine (C-X-C motif) receptor 3, CX3C chemokine receptor 1, toll-like receptor (TLR)1, TLR7, TLR9, TLR12, transforming growth factor-β, HMGB1, S100A8, S100A9, and galectin-3 were determined using forward and reverse primer pairs detailed in Online Table I and normalized to 18s rRNA expression using the $\Delta\Delta C_T$ comparative method.[3]

Survival Splenectomy and Splenocyte Adoptive Transfer

In a separate subgroup, male (CD45.2) C57BL/6J mice (n=36) underwent coronary ligation or sham operation. Eight weeks later, survival splenectomy (or, in some mice, sham abdominal surgery) was performed using standard surgical techniques.[29] Briefly, mice were anesthetized with tribromoethanol (0.25 mg/g IP), and anesthesia was maintained with 1% isoflurane as needed. After sterilizing the surgical area, ≈1 cm incision was made in the left subcostal region, and the peritoneum was opened to exteriorize the spleen. The spleen was retracted away from the pancreatic tail, the splenic bundle was ligated at the hilum using 8.0 prolene ligature, and the spleen was removed intact. For sham operations, the splenic bundle and spleen were left intact. The procedure required ≈10 to 15 minutes to complete; totality of splenectomy was ensured by close examination at the time of operation and confirmed during postmortem examination. Splenocytes from sham-operated and HF mice were used for adoptive transfer studies described below. Splenectomized mice (and sham abdominal surgery controls) were subsequently followed for 8 more weeks with serial echocardiography.

For adoptive transfer studies, splenocytes were prepared as described previously.[30] Briefly, single-cell suspensions were prepared from spleens isolated from sham-operated (n=8) and HF mice (n=7). The erythrocytes were lysed with RBC lysis buffer (eBiosciences). Single-cell suspensions were then layered on Ficoll-Paque (GE Healthcare) gradient and centrifuged at 2000*g* for 20 minutes to separate mononuclear cells and exclude granulocytes and residual erythrocytes. Mononuclear cells were collected, washed 3 times with sterile PBS, and resuspended in sterile PBS. Cells were then pooled from either sham or HF mice and resuspended in 5 mL PBS. Mononuclear cells were injected (≈17×10^6 cells in 100 μL PBS per animal via tail vein) into naive CD45.1 C57BL/6J mice (7 mice receiving sham splenocytes and 7 mice receiving HF splenocytes).

As an additional control for adoptive transfer, we also isolated splenocytes from CD45.2 C57BL/6J male mice (6–8 weeks) treated with either lipopolysaccharide (LPS) to induce systemic inflammation or PBS control. LPS (0.4 mg/kg) or PBS (0.2 mL) was injected intraperitoneally daily for 2 consecutive days (n=5 per group). Spleens were aseptically harvested 24 hours after the last intraperitoneal dose, and the mononuclear cell population was isolated and injected via tail vein into naive CD45.1 C57BL/6 recipient mice (n=7 per group receiving either LPS splenocytes or PBS splenocytes) as described above.

Statistical Analysis

Continuous data are summarized as mean±SD. Statistical comparisons were performed using the unpaired Student *t* test when comparing 2 groups. For comparisons of >2 groups, 2-way ANOVA was used with Bonferroni post-test to adjust for multiple comparisons. A *P* value <0.05 was considered statistically significant.

Results

Profound Structural Remodeling in the Heart 8 Weeks After Coronary Ligation

Four weeks after coronary ligation, mice exhibited significant pathological cardiac remodeling and hemodynamic signs of HF.[3,15] Here, we evaluated mice at 8 weeks to ensure the establishment of chronic ischemic HF. Typical M-mode ECGs and ventricular sections from sham-operated and HF mice (Online Figure IA), and histological sections of remote (noninfarcted) myocardium stained with Masson trichrome and wheat germ agglutinin (Online Figure IB), demonstrated substantial myocardial scarring, LV dilatation, LV systolic dysfunction, and increased fibrosis and myocyte size in HF mice. Group data (Online Figure IC) confirmed significantly increased LV end-diastolic and end-systolic volume, reduced LV ejection fraction, and increased (≈2-fold) remote zone fibrosis and myocyte area. Normalized heart and lung weights were also increased. These findings indicated marked LV remodeling and pulmonary edema in HF mice.

Activated M1 Polarized Macrophages Infiltrate the Failing Heart

Activated macrophages were defined as cells with dual expression of CD11b (Mac-1) and F4/80 surface markers.[20,21] As seen in Figure 1A, as compared with sham, failing hearts exhibited a significant increase in both overall mononuclear cells and infiltrating activated macrophages (19.2±1.9 versus 10.9±2.9%; *P*=0.033). Augmented tissue macrophages were further confirmed by Mac-1 immunostaining (Figure 1B), which revealed a ≈5-fold increase in macrophages in failing hearts compared with sham (*P*<0.001). Lin2 negativity (see Methods section) and CD206 expression were used to subclassify macrophages as either M1 (proinflammatory; Lin2$^-$CD11b$^+$F4/80$^+$CD206$^-$) or M2 (anti-inflammatory; Lin2$^-$CD11b$^+$F4/80$^+$CD206$^+$) by flow cytometry. As seen in Figure 1C,

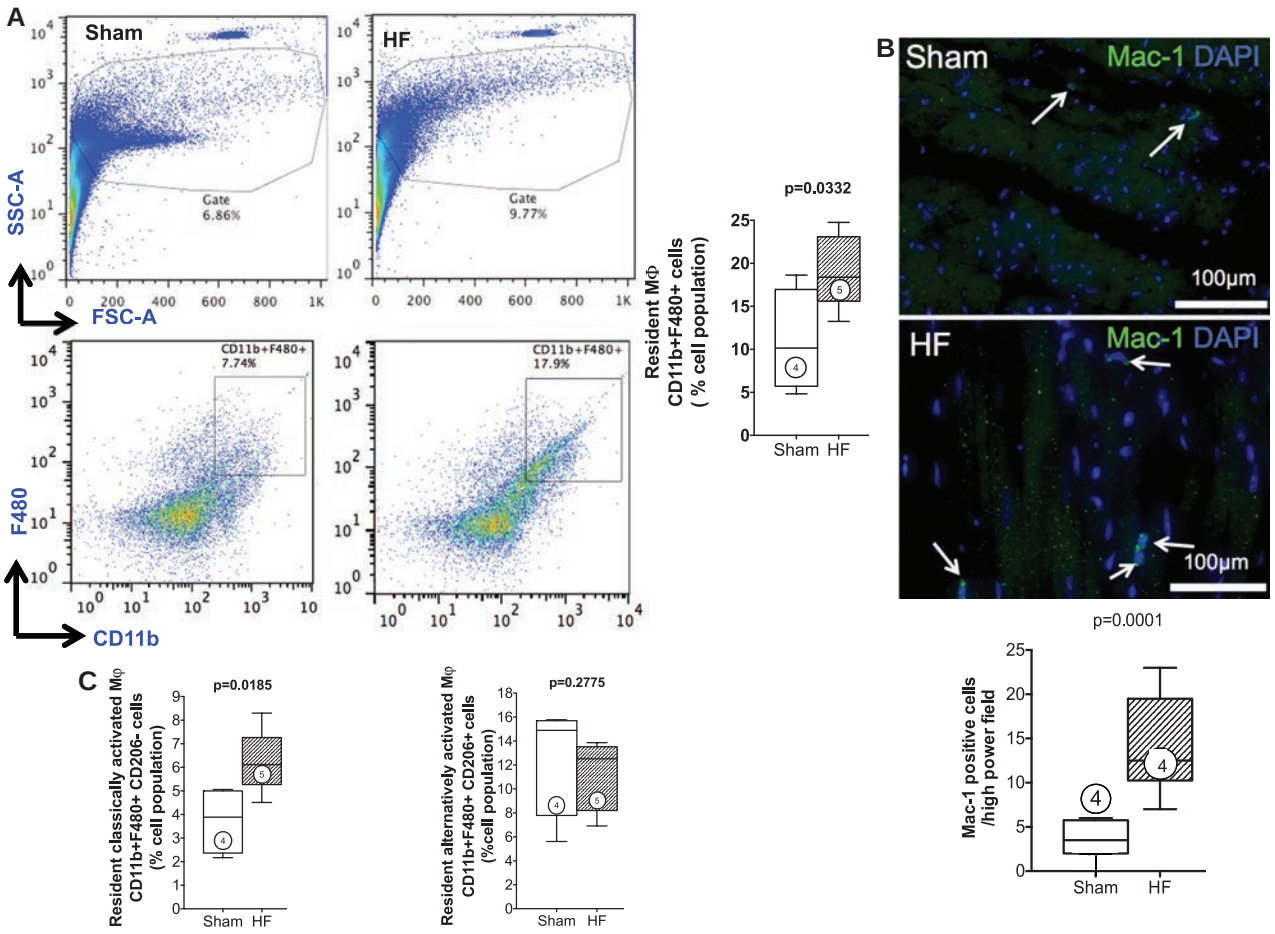

Figure 1. Activated macrophages infiltrate the failing heart. **A**, Cardiac mononuclear cells were isolated on tissue digestion and gradient centrifugation purification. Representative forward and side scatter profiles and live cell gates from a sham and HF heart (**top**). Identification of Lin2$^-$ (defined in text) CD11b$^+$F480$^+$ cells, expressed as a percentage of total live cells, and corresponding group data from sham and HF hearts (**bottom**). FSC indicates forward scatter; and SSC, side scatter. **B**, Representative Mac-1 immunostains in sham and HF hearts and corresponding quantification of Mac-1$^+$ cells (arrows). **C**, Flow cytometric quantification of classically activated M1 (Lin2$^-$CD11b$^+$F4/80$^+$CD206$^-$) and alternatively activated M2 (Lin2$^-$CD11b$^+$F4/80$^+$CD206$^+$) macrophages in sham and HF hearts. Mϕ indicates macrophage; n=4 to 5 per group.

both sham and failing hearts exhibited a greater abundance of tissue M2 macrophages in relation to M1 macrophages, consistent with previous studies.[31] M1 macrophages significantly increased in the failing heart compard with sham (6.2±0.6 versus 3.8±0.7%; P=0.019), whereas there was no change in M2 macrophages (P=0.28), thus favoring a proinflammatory milieu. In support of this, HF mice (compared with sham) exhibited significant (or near significant) elevations of circulating proinflammatory IFN-γ, IL-6, and MCP-1 in serum (Online Figure II). No differences among groups were observed for serum levels of IL12p70, TNFα, and IL-10.

cDCs and pDCs Increase in the Failing Heart

CD11c$^+$ DCs are antigen-presenting cells categorized as classical and nonclassical DCs.[22] cDCs include migratory DCs (present in most organs, including the heart), which activate immune responses after detection of danger signals, and lymphoid tissue-resident DCs, which do not migrate but collect and process antigens in 1 lymphoid organ throughout their lifespan.[22] Nonclassical DCs include pDCs that are present in an immature form at steady state, but they mature with dendritic form and costimulatory molecule expression on inflammatory activation.[6,22,26] As seen in Figure 2A, CD11c immunostaining revealed distinctly increased tissue DC infiltration in the interstitium of the failing heart (border and remote zone) as compared with sham. DC subsets in the heart were quantified by flow cytometry using Lin1 negativity (see Methods section), with cDCs identified as Lin1$^-$CD11c$^+$B220$^-$, and pDCs as Lin1$^-$CD11c$^{+/low}$B220$^+$.[23,24] pDCs were further classified as CD86^{low} and CD86^{hi}, to indicate immature and mature pDCs, respectively.[26] Both DC populations increased in the failing heart, cDCs by ≈1.4-fold (P=0.023) and pDCs by ≈4.3-fold (P=0.012), compared with sham (Figure 2B). Moreover, pDCs over a range of maturation stages were present in the failing heart. As seen in Figure 2C, the number of mature CD86^{hi} and immature CD86^{low} pDCs in sham hearts was very low. However, both pDC populations were markedly increased in HF hearts as compared with sham (≈9-fold higher CD86^{hi} pDCs, P=0.009; ≈22-fold higher CD86^{low} pDCs, P<0.001).

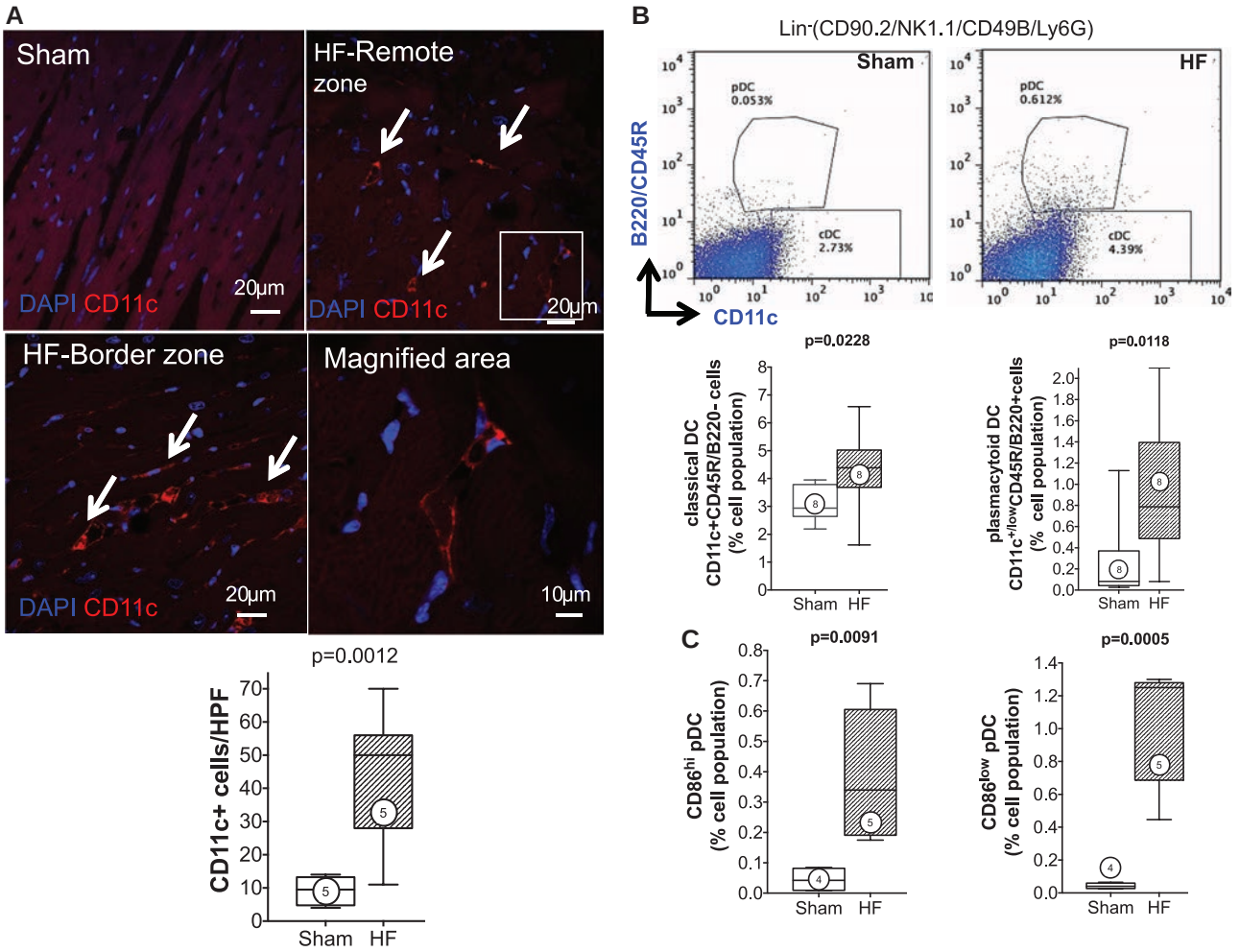

Figure 2. Infiltrating dendritic cells (DCs) are increased in the failing heart. **A**, Representative confocal images of CD11c immunostained sections from sham and HF hearts (remote zone) and corresponding group data. The arrows indicate infiltrating CD11c$^+$ DCs; n=5 per group. **B**, Representative scatter plots for Lin1$^-$ (defined in text) cardiac mononuclear cells further separated into CD11c$^+$B220$^-$ classical DCs (cDCs) and CD11c$^{+/low}$B220$^+$ plasmacytoid DCs (pDCs), expressed as a percentage of total live cells, together with quantitative group data for cDC and pDC populations in sham and HF hearts. N=8 per group. **C**, Flow cytometric quantification of CD86^{hi} and CD86^{low} pDCs in sham and HF hearts. N=4 to 5 per group.

Splenic Remodeling Is Prominent in Chronic HF

Masson trichrome stains of the spleen revealed striking alterations of the splenic architecture in HF. As seen under low power (Figure 3A), the HF spleen exhibited greater numbers of white pulp follicles (primarily composed of lymphocytes), with greater variability and irregularities of follicular size and shape and greater numbers of large germinal centers as compared with spleens from sham-operated mice. Higher-power views revealed a striking increase in size of the marginal zone surrounding the white pulp, a site that plays an important role in antigen screening and processing.[32] The changes in tissue architecture suggested immune activation and heightened antigen processing in the spleen.[32] Additionally, there was reduced mononuclear cell abundance in the red pulp, especially the SRP, in HF spleens.

To quantify monocytes/macrophages and DCs in the spleen, flow cytometry and immunostaining were performed. As seen in Figure 3B, CD11b/Mac-1 and F4/80 immunostains revealed ≈3.4-fold fewer activated monocytes in the spleens of HF mice as compared with sham, primarily in the red pulp and SRP. This was confirmed by flow cytometry of the splenic mononuclear cell population (Figure 3C), which revealed a significant (P=0.0011) ≈2-fold reduction in $CD11b^+F4/80^+$ cells in HF spleens. These changes were primarily related to proinflammatory ($CD11b^+F4/80^+Gr\text{-}1^{hi}$) monocytes without significant change in anti-inflammatory ($CD11b^+F4/80^+Gr\text{-}1^{low}$) monocytes. In contrast to activated monocytes, lymphoid tissue-resident DC populations were markedly increased in the spleens of HF mice. As seen in Figure 4A and 4B, both $CD11c^+B220^-$ cDC and $CD11c^{+/low}B220^+$ pDC populations were augmented in HF spleens. Increased splenic pDCs in HF were also observed using Siglec-H as a pDC marker (Online Figure III).

In lymphoid organs, $CD8^+$ and $CD8^-$ cDCs differ in their efficiency for antigen cross-presentation to T-cells.[6,22,33] As seen in Figure 4C, there was a significant ≈1.8-fold increase in both $CD8^+$ and $CD8^-$ cDCs in spleens from HF mice as compared with sham, together with significantly increased numbers of $CD4^+$ and $CD8^+$ T-cells (Online Figure IV). Importantly, although both $CD8^+$ and $CD8^-$ cDCs prime T-cell responses, $CD8^+$ DCs have a greater propensity to stimulate $CD8^+$ cytotoxic T-cells[6,33] and Th-1 $CD4^+$ helper T-cells[34] that would promote a proinflammatory milieu. In addition to increased splenic DC abundance in HF, CD11c immunostaining revealed a striking spatial redistribution of DCs (Figure 4D). In sham-operated mice, splenic $CD11c^+$ DCs were primarily seen in the marginal zone. In contrast, in HF spleens, DCs were localized within the white pulp and often in germinal centers, suggesting a critical role for DCs in the heightened antigen processing occurring in HF.

Augmented Circulating cDCs and Proinflammatory Monocytes in HF

HF mice exhibited a marked ≈2-fold increase in circulating $CD11b^+F4/80^+$-activated monocytes (P=0.01) as compared with sham (Figure 5A). These changes were again related to proinflammatory monocytes, analogous to the polarity of tissue macrophages in the failing heart (Figure 1) and consistent with the systemic elaboration of proinflammatory mediators such as MCP-1 (Online Figure II). Notably, circulating anti-inflammatory monocytes decreased substantially in HF mice. cDCs and pDCs were also detected in the circulation of sham and HF mice (Figure 5B). Both circulating $CD8^+$ and $CD8^-$ cDCs were increased ≈2- to 3-fold in HF mice as compared with sham, whereas circulating pDCs were similar between the groups. In contrast, BM from HF mice exhibited significantly (≈1.4-fold) increased pDCs, but no change in cDCs or activated monocytes when compared with sham BM (Online Figure V).

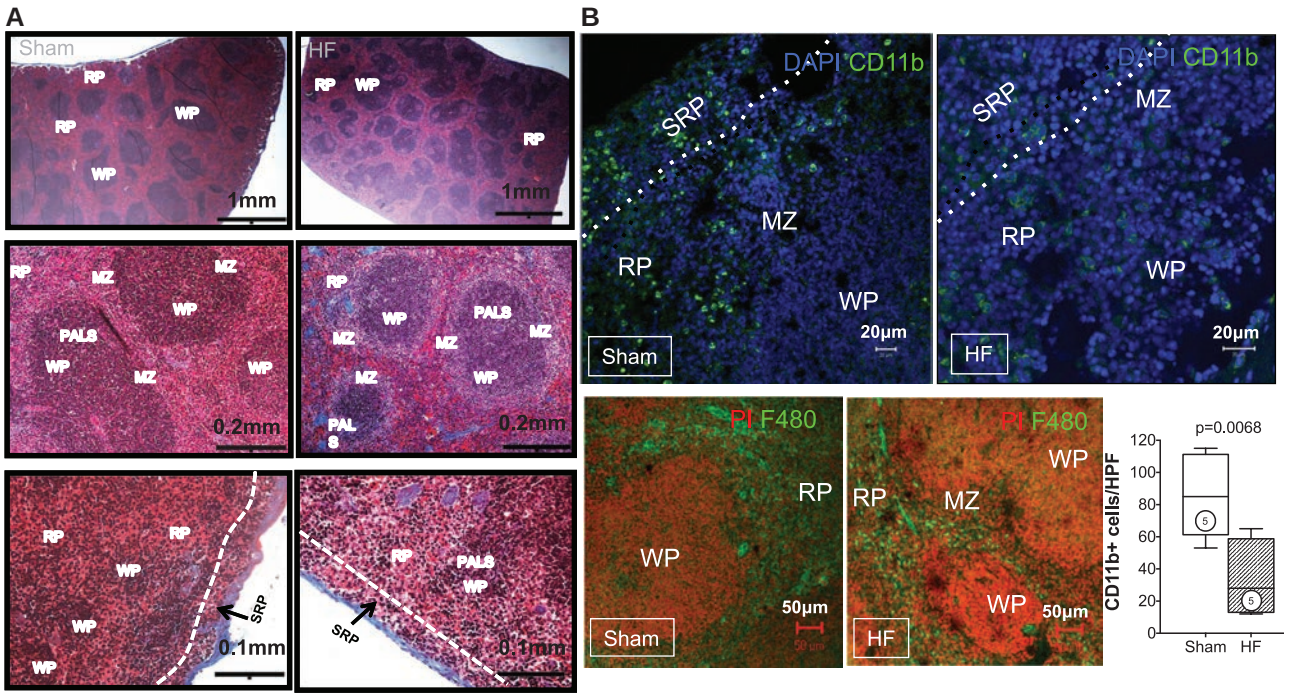

Figure 3. Continued

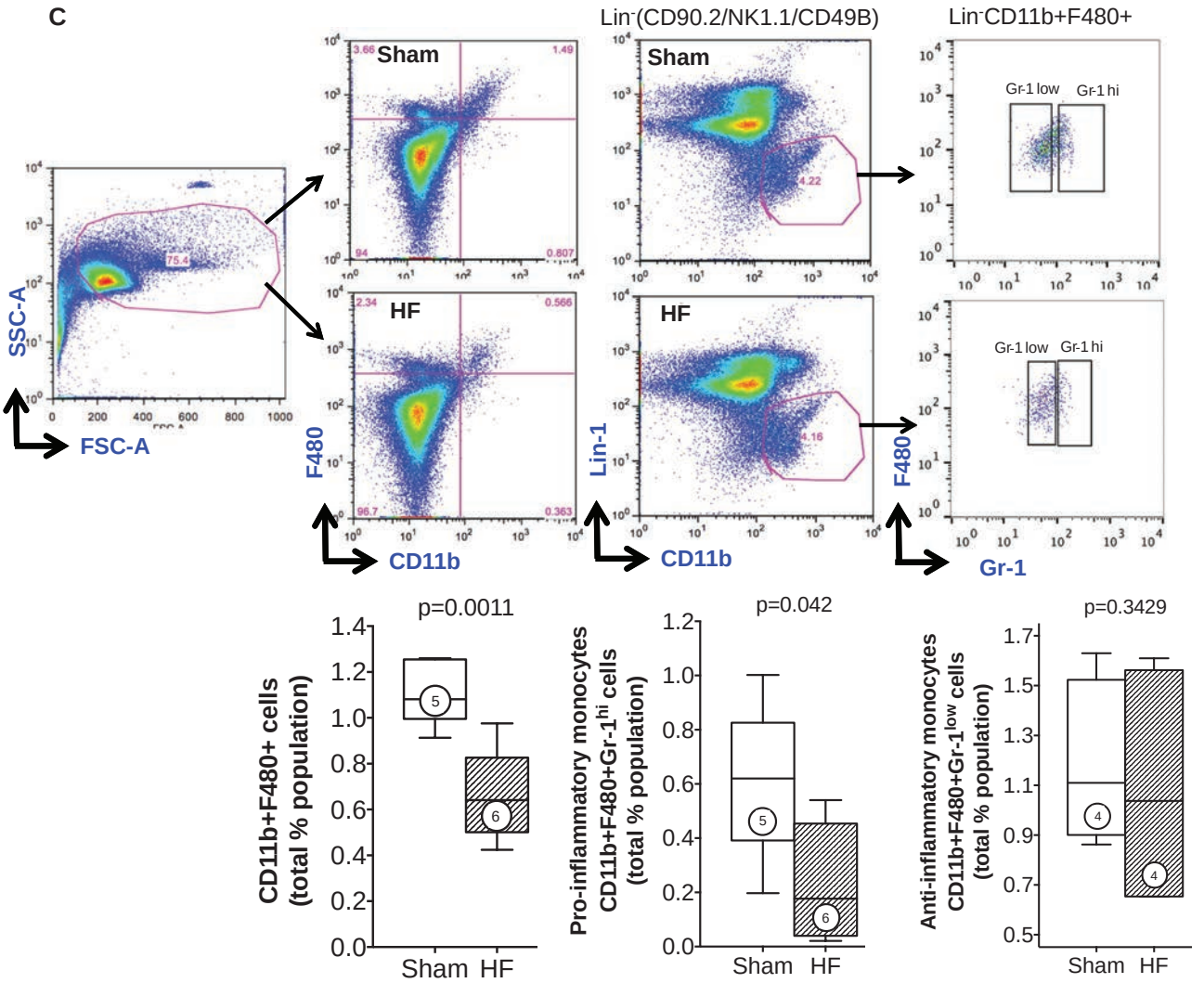

Figure 3. Splenic remodeling in heart failure. A, Representative Masson trichrome stains of spleens from sham-operated and heart failure (HF) mice. The low-power views (**top**) depict increased white pulp (WP) follicles with greater number of large germinal centers (clear areas in the WP) in the spleen from HF mouse. The higher-power views (**middle**) illustrate the increased size of the marginal zone (MZ) surrounding the WP in the HF spleen. The bottom panels highlight the subcapsular red pulp (SRP), which exhibits fewer mononuclear cells in HF as compared with sham. PALS indicates periarteriolar lymphoid sheath. **B**, Representative confocal images of CD11b$^+$ SRP monocytes (**top**) and F4/80$^+$ monocytes (**bottom**) in the red pulp of sham and HF spleens, together with quantitative group data for CD11b$^+$ cells in the SRP. **C**, Representative live cell gates and scatter plots from sham and HF spleens identifying CD11b$^+$F480$^+$ cells, further subdivided by low or high Gr-1 expression (percentage of total live cells), and corresponding group data. N=4 to 6 per group.

Spleen Regulates the Progression of Pathological LV Remodeling in Chronic HF

Our data indicated global proinflammatory alterations of the antigen-presenting cell network in HF. As the largest lymphoid organ in the body, the spleen would be expected to be the critical lynchpin for their pathogenesis and, by analogy, for the progression of cardiac remodeling. To examine this as a proof-of-principle, 2 approaches were used. First, splenectomy (or sham splenectomy) was performed in mice with HF 8 weeks post–coronary ligation, and the effects on LV remodeling were evaluated 8 weeks later (Figure 6A). Splenectomy in sham-operated mice did not induce any changes in LV size or function. Figure 6B depicts representative M-mode ECGs from 1 mouse at baseline, 8 weeks postligation (HF), and 16 weeks postligation/8 weeks postsplenectomy (HF/splenectomy). LV enlargement and dysfunction significantly improved postsplenectomy. Group data (Figure 6C) confirmed that splenectomy in HF, over a period of 8 weeks, induced significant (P<0.05) reductions in end-diastolic volume and end-systolic volume and improvement (22% relative change, 8% absolute change) in LV ejection fraction, indicating reversal of pathological remodeling, whereas HF mice with sham abdominal surgery at 8 weeks continued to show progressive LV remodeling and functional decline. Moreover, cardiac CD11b and CD11c immunostaining revealed a profound ≈3-fold reduction in tissue macrophages and DCs in the failing heart after splenectomy (Figure 6D). Also, as illustrated in Online Figure VI, splenectomy did not reduce serum levels of TNF, MCP-1, IL-6, IL12p70, and IFN-γ in HF mice (IL-6 levels were actually mildly increased after splenectomy). Taken together, this suggests that the improved LV remodeling after splenectomy was not simply related to changes in

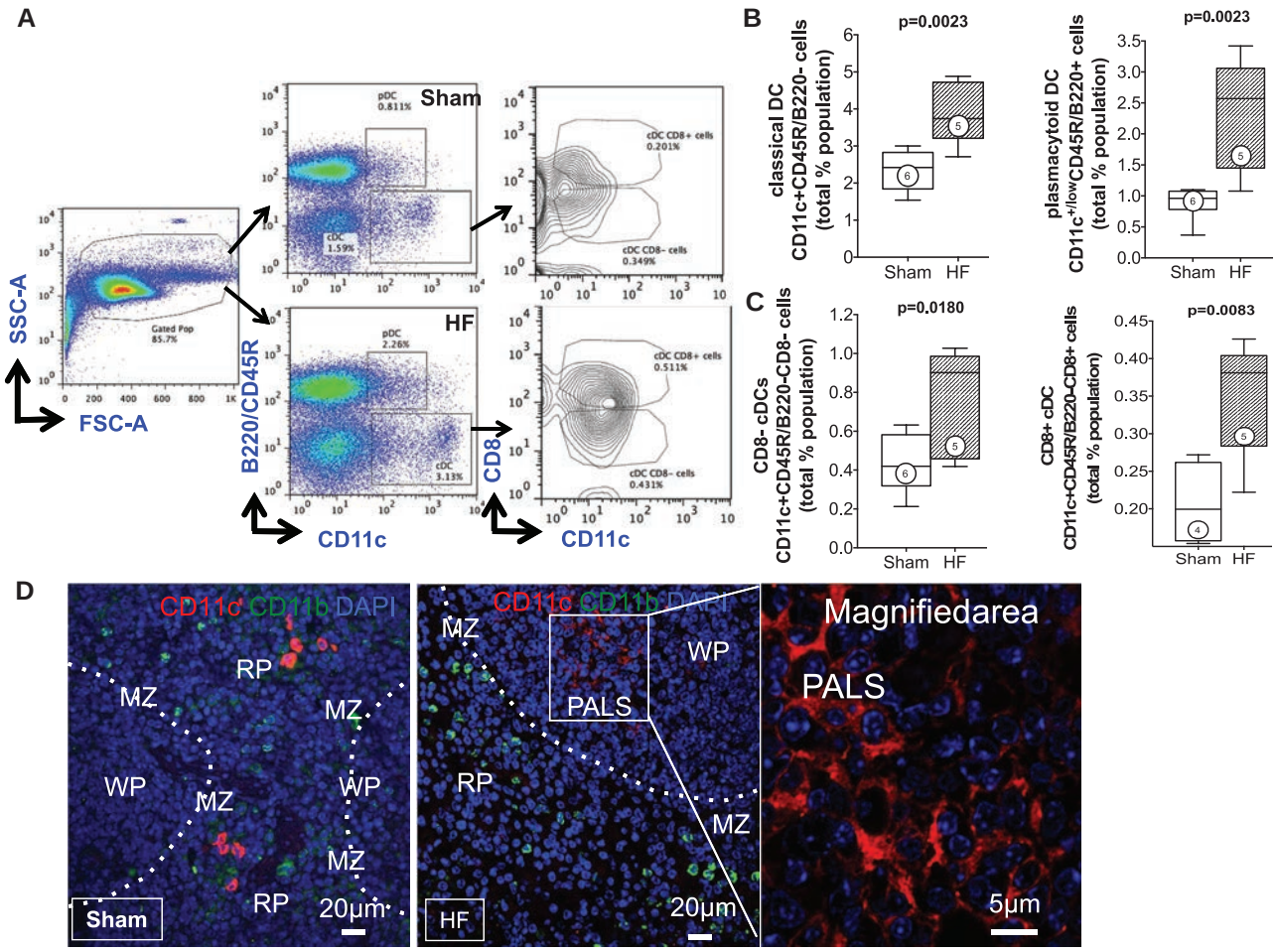

Figure 4. Remodeling of the splenic dendritic cell (DC) population in heart failure (HF). **A**, Representative scatter plots for splenic mononuclear cells and live cell gates, with subsequent identification of Lin1⁻ CD11c⁺B220⁻ classical DCs (cDCs) and CD11c⁺B220⁺ plasmacytoid DCs (pDCs), and further subdivision of cDCs as CD8⁺ or CD8⁻ cells. **B** and **C**, Quantitative group data for cDCs and pDCs, and CD8⁺ and CD8⁻ cDCs, expressed as a percentage of total live cell population in sham and HF spleens. N=4 to 6 per group. **D**, Representative confocal images of CD11c⁺ DCs in sham and HF spleens demonstrating prominent spatial redistribution of DCs to the white pulp germinal centers in the HF spleen.

circulating cytokines, but rather to loss of splenic mobilization and subsequent diminished tissue infiltration of inflammatory cells.

Second, we performed adoptive transfer of mononuclear splenocytes isolated from either sham-operated or HF (CD45.2) mice into naive (CD45.1) syngeneic C57Bl/6 mice and serially evaluated LV remodeling during an 8-week period (Figure 7A). Flow cytometry revealed persistence of donor splenocytes in the peripheral blood of recipients at a level of ≈15% by 1 week and <1% to 2% by 2 weeks post-transfer (Online Figure VII). Mice that received splenocytes from sham-operated mice exhibited no appreciable changes in LV size or ejection fraction during an 8-week period after cell transfer (Figure 7B and 7C). However, mice that received splenocytes from HF mice had significant (P<0.05) LV dilatation (≈30% and ≈60% increase in end-diastolic volume and end-systolic volume, respectively) and LV ejection fraction decline evident by 8 weeks. Analogous to HF mice with splenectomy, serum levels of TNF, MCP-1, IL-6, IL12p70, and IFN-γ were similar between mice receiving HF splenocytes and sham splenocytes (Online Figure VIII), suggesting that the remodeling responses were not secondary to high systemic cytokines. Moreover, to exclude a nonspecific response, we performed parallel experiments using splenocytes from mice given intraperitoneal LPS (or PBS control) for 2 days. Although this LPS regimen significantly augmented circulating proinflammatory CD11b⁺F4/80⁺Gr-1⁺ cells as compared with PBS-treated mice (Online Figure IXA), adoptive transfer of LPS splenocytes (or PBS splenocytes) had no discernible effects on LV size or systolic function (Online Figure IXB; Figure 7D), suggesting that the HF splenocyte response was specific to the HF disease state itself rather than nonspecific inflammation.

HF Splenocytes Express Inflammatory Mediators and Alarmins, and Home to the Heart to Induce Pathological Injury

Gravimetric analysis (Figure 7E) revealed increased heart and lung weights in HF splenocyte recipient mice, as compared with sham splenocyte recipients, indicative of cardiac hypertrophy and lung edema. Peripheral blood flow cytometry 8 weeks post-transfer also revealed augmented

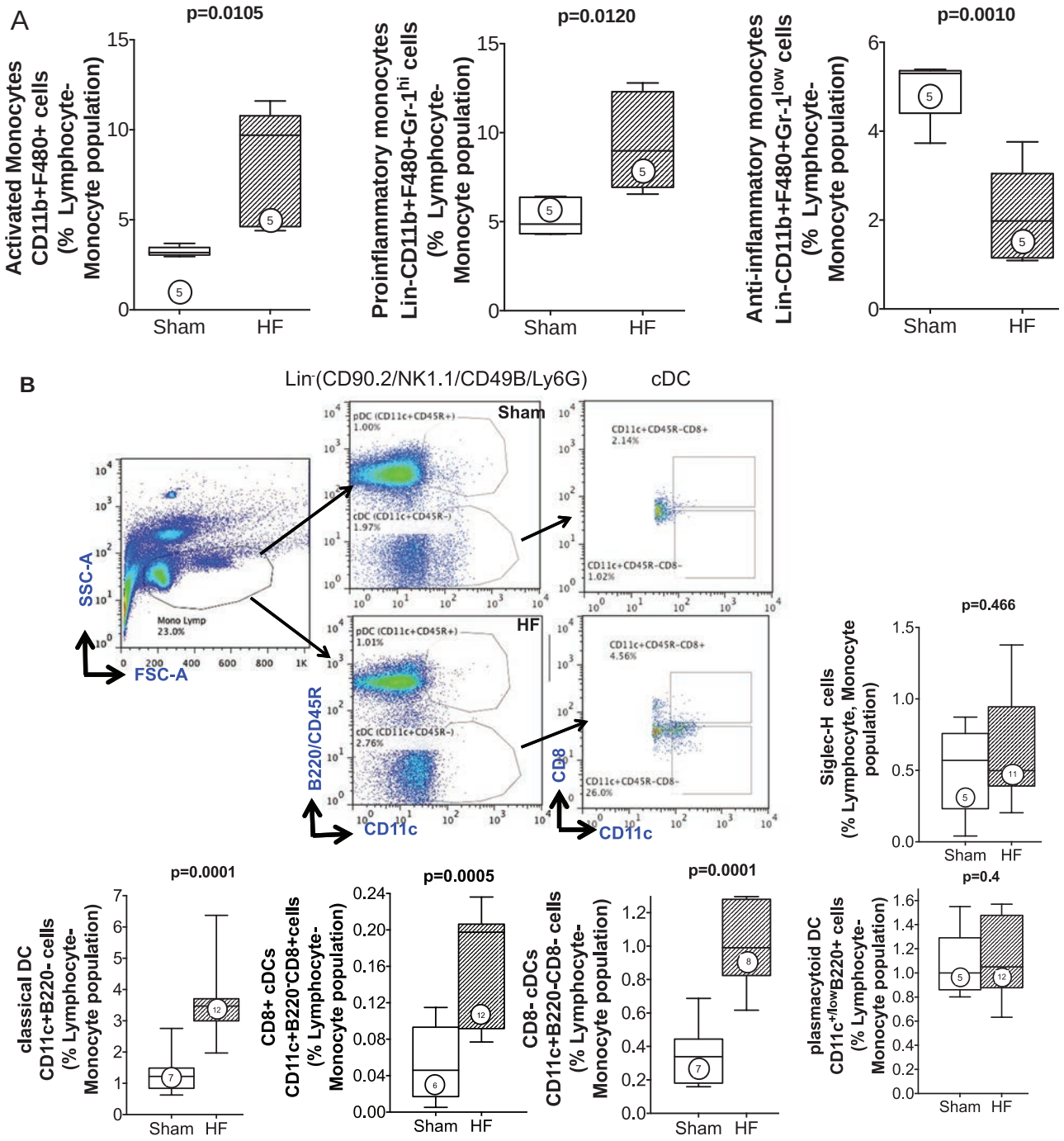

Figure 5. Altered circulating mononuclear phagocytes in heart failure (HF). A, Lin2⁻CD11b⁺F4/80⁺ monocytes were identified from the monocyte–lymphocyte gate of peripheral blood leukocytes and further subdivided as high or low Gr-1–expressing cells (pro- and anti-inflammatory monocytes, respectively). Quantitative group data for circulating monocyte subsets in sham and HF mice are shown; n=5 per group. **B**, Schema for flow cytometric identification of circulating Lin1⁻CD11c⁺B220⁻ classical DCs (cDCs) and CD11c⁺B220⁺ plasmacytoid DCs (pDCs), and CD8⁺ and CD8⁻ cDCs, expressed as a percentage of the monocyte–lymphocyte gate of peripheral blood cells determined from side and forward scatter (SSC, FSC) plots as shown, together with quantitative group data for the same in sham and HF mice. In parallel studies, peripheral blood pDCs were alternatively identified as Siglec-H⁺ cells and expressed as a percentage of the monocyte–lymphocyte gate. N=5 to 12 per group.

activated CD45.1 monocytes, indicating reproduction of chronic inflammation in recipients (Figure 7F). Moreover, as compared with sham splenocyte recipient mice, the spleens of HF splenocyte mice were hypertrophied and exhibited histological changes indicative of heightened antigen processing similar to that observed in mice with HF (Figure 7G). Histological analysis of HF splenocyte recipient hearts revealed augmented interstitial fibrosis as compared with sham splenocyte recipient hearts (Figure 8A); fibrotic foci often coincided with retained CD45.2⁺ donor cells. These hearts also exhibited a ≈10-fold increase in cardiomyocyte apoptosis (Figure 8B), suggesting HF

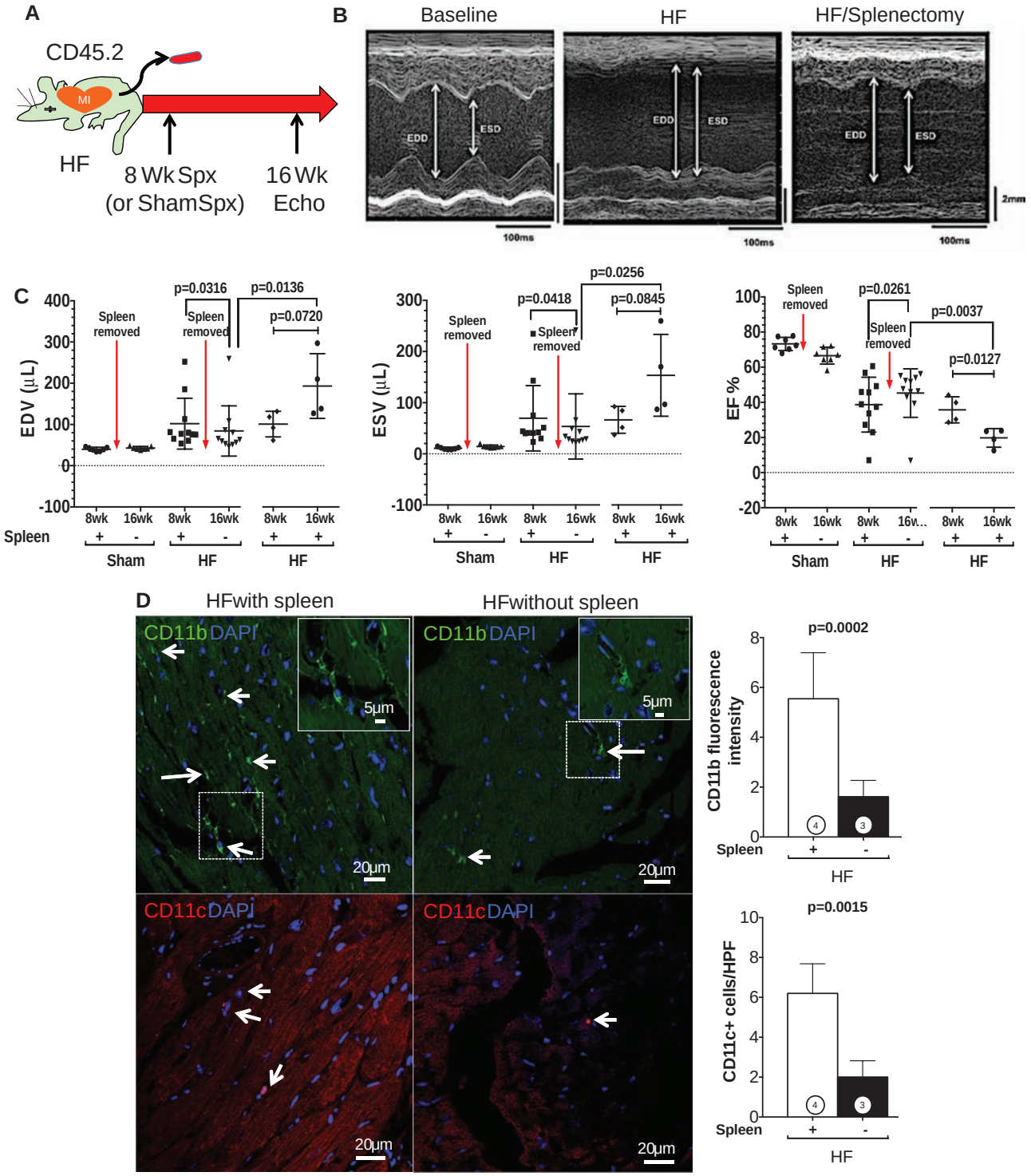

Figure 6. The spleen influences pathological cardiac remodeling in heart failure (HF). A, Schema for splenectomy studies in mice with chronic HF. Splenectomy (or sham abdominal surgery) was performed in HF mice 8 weeks after coronary ligation (or sham operation), and remodeling was assessed by echocardiography over an additional 8 weeks. **B**, M-mode ECGs from 1 mouse at baseline, 8 weeks postligation (HF), and 16 weeks postligation/8 weeks postsplenectomy (HF/splenectomy). **C**, Quantitative group echocardiographic data for left ventricular (LV) end-diastolic and end-systolic volume (EDV and ESV) and LV ejection fraction (EF) in sham operated and ligated HF mice 8 weeks after splenectomy (n=7 sham mice; n=11 HF mice) or sham abdominal surgery (n=4 HF mice). **D**. Representative confocal images of CD11b (for macrophages, arrows) and CD11c (for DCs, arrows) immunostained heart sections from HF mice (16 weeks postligation) with or without splenectomy at 8 weeks and corresponding quantification (n=3–4 per group).

splenocyte–induced cell loss as a potential trigger for myocardial fibrosis. To confirm cardiac homing of HF splenocytes, we performed immunostaining for CD169, a marker for splenic metallophilic marginal zone macrophages.[35] HF splenocyte recipient hearts, but not sham splenocyte recipient hearts, harbored multiple foci of CD45.2^{+}CD169^{+} cells

in the perivascular and interstitial regions (Figure 8C). We also observed CD169^{+} macrophages in the border zone of failing hearts 8 weeks after coronary ligation, but not in sham-operated hearts (data not shown). Hence, mononuclear splenocytes activated in HF home to the heart to induce tissue injury and remodeling and retain memory sufficient to induce similar inflammation and long-term pathological remodeling in otherwise naive hearts.

We examined inflammatory gene expression in splenocytes and levels of splenic alarmins as potential mechanisms for immune cell–mediated injury. As illustrated in Online Figure X, as compared with sham, splenocytes from HF mice exhibited significantly increased expression of several proinflammatory cytokines/mediators (eg, TNF, IL-2, IL-5, IL-6, iNOS, IFN-γ), chemokine receptors/ligands (eg, C-C chemokine receptor type 2, CX3C chemokine receptor 1, chemokine [C-C motif] ligand 5, chemokine [C-X-C motif] receptor 3), and pattern recognition receptors (eg, TLR-7, TLR-9, TLR-12) of signal importance in the activation of DCs.[36] In contrast, of the anti-inflammatory mediators examined (IL-4, IL-10, IL-13, transforming growth factor-β), only IL-10 was upregulated. Hence, HF splenocytes are potently activated and serve as sources of inflammatory mediators that can initiate or amplify tissue injury.

Pattern recognition receptor upregulation, cell homing to the heart, and the capacity to reproduce systemic inflammation and cardiac injury and remodeling on HF splenocyte adoptive transfer suggest previous priming of the transferred immune cells by cardiac antigens. Potential candidates for the latter include damage-associated molecular patterns or alarmins and TLR ligands released on cardiac injury that can activate innate immune cells both locally and globally.[37,38] As shown in Online Figure XIA, immunostaining of HF spleens revealed robustly increased levels of both intracellular and extracellular HMGB1, a prototypical alarmin, in the white pulp, marginal zone, and SRP, suggesting ongoing HMGB1 antigen presentation to T-cells. HF splenocytes themselves further exhibited significant upregulation of several alarmins, including HMGB1, S100A8, S100A9, and galectin-3 (Online Figure XIB), which can amplify the inflammatory response.[37] Moreover, adoptively transferred HF splenocytes were also intermittently observed to express HMGB1 robustly in recipient hearts (Online Figure XIC). Taken in totality, the adoptive transfer studies provide direct evidence for activated splenocytes as disease mediators in HF, as part of a pathophysiologically relevant cardio-splenic axis that is both necessary and sufficient for the progression of LV remodeling.

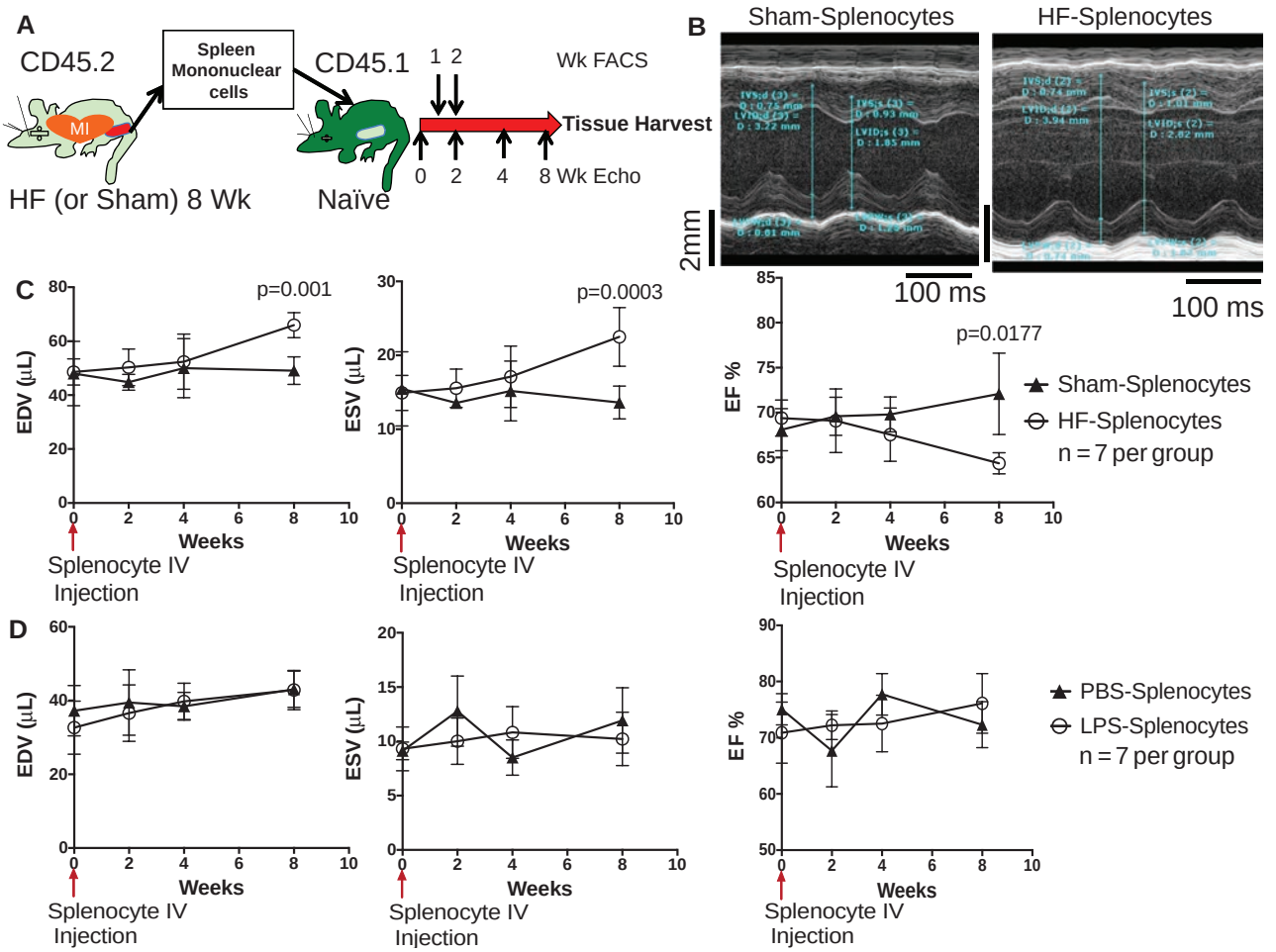

Figure 7. Continued

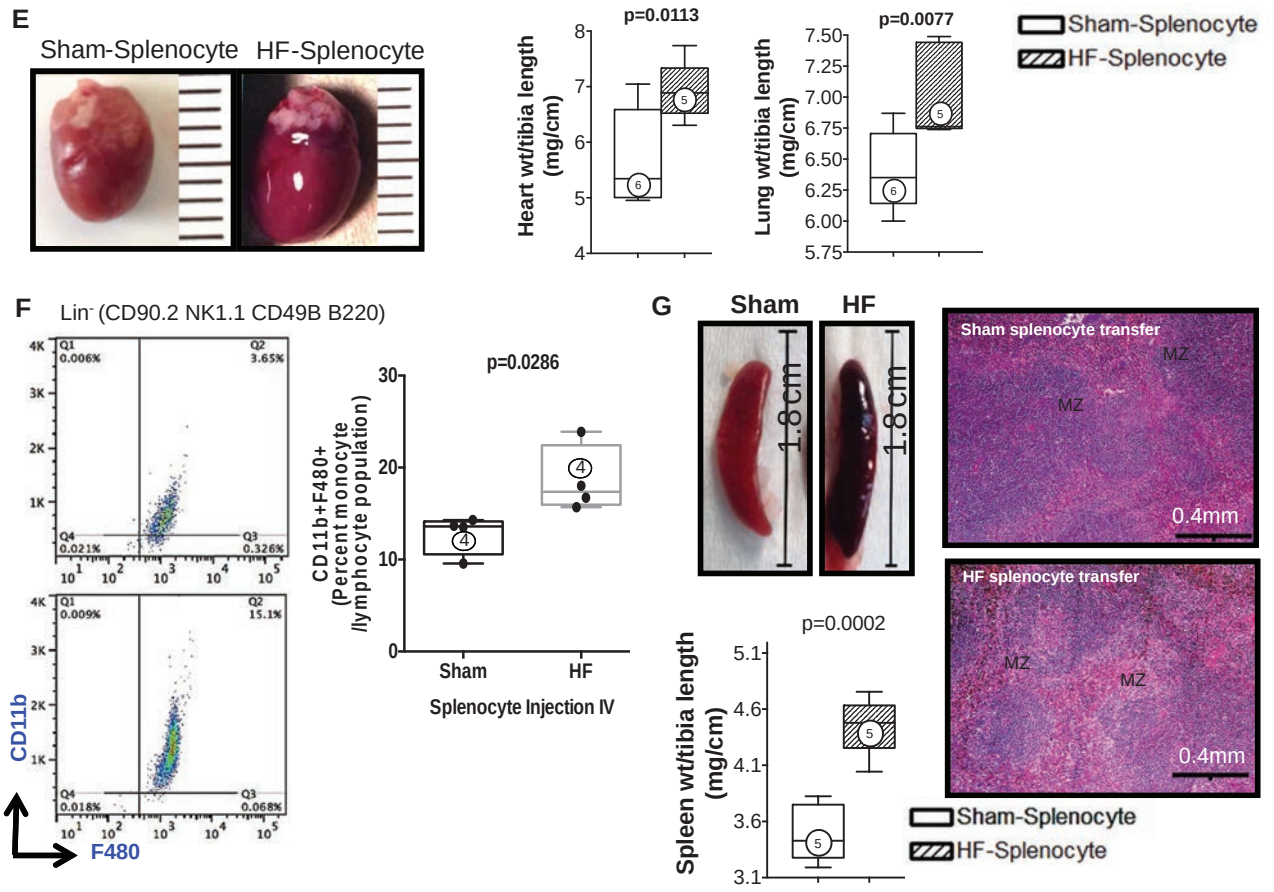

Figure 7. Heart failure (HF)-derived splenocytes induce pathological cardiac remodeling on adoptive transfer. **A**, Schema for splenocyte adoptive transfer experiments. Splenocytes were isolated from CD45.2 sham and HF mice 8 weeks after coronary ligation or sham operation and transferred to syngeneic CD45.1 mice. Recipient mice were then followed for an 8-week period. **B**, M-mode ECGs from recipient mice 8 weeks after receiving splenocytes from sham or HF mice. **C**, Serial group echocardiographic data for end-diastolic volume (EDV), end-systolic volume (ESV), and ejection fraction (EF) during the 8-week follow-up period after cell transfer (n=7 per group). **D**, Similar echocardiographic data in parallel groups of mice after adoptive transfer of splenocytes derived from donors treated with either lipopolysaccharide (LPS) or PBS control (n=7 per group). **E**, Representative hearts from mice receiving HF or sham splenocytes and corresponding heart and lung gravimetric group data. **F**, Flow cytometry scatter plots and quantification of circulating $CD11b^+F4/80^+$ monocytes in recipient mice 8 weeks after cell transfer. **G**, Examples of spleens harvested from mice receiving HF or sham splenocytes, corresponding spleen gravimetry, and representative trichrome-stained histological sections from the same. N=4 to 6 per group (**E–G**).

Discussion

There are several novel findings in this study. First, there are profound alterations of the mononuclear phagocyte network in established ischemic HF that encompass the failing heart, spleen, peripheral blood, and BM and form the foundation for chronic inflammation in this disease. These are comprised of: (1) increased proinflammatory macrophages and monocytes in the failing heart and peripheral blood, together with a reduction in the activated monocyte reservoir in the spleen, (2) augmented cDCs and pDCs in both the failing heart and spleen and increased cDCs and pDCs in the blood and BM, respectively, and (3) increased levels of both $CD8^+$ and $CD8^-$ cDC subtypes in the spleen and blood. Augmented circulating levels of IFN-γ, MCP-1, and IL-6 accompanied these immune cell profiles. Second, there is profound splenic remodeling in HF, indicative of ongoing, heightened antigen processing. This occurred in concert with robust expression of alarmins and proinflammatory mediators and augmented splenic $CD4^+$ and $CD8^+$ T-cell populations, consistent with heightened T-cell activation and differentiation secondary to antigen–MHC presentation by DCs. Third, the spleen has an obligatory role in the progression of cardiac remodeling and inflammation in chronic HF, because splenectomy reversed remodeling and attenuated tissue macrophage and DC infiltration. Fourth, HF-derived mononuclear splenocytes, not otherwise activated ex vivo, home to the heart and induce long-term cardiac remodeling and dysfunction, systemic inflammation, and splenic remodeling akin to HF in previously normal mice. These data indicate that mononuclear splenocytes in chronic HF are highly activated, potentially in response to cardiac-derived alarmins, and traffic to the heart to induce immune cell–mediated injury, and that this capacity is retained on adoptive transfer into naive animals. Taken together, we conclude that activation of mononuclear phagocytes is indispensable for the progression of pathological remodeling and that the splenic microenvironment in HF plays a critical role in this process.

Altered Inflammatory Cell Network in HF

Recent studies have established a critical role for monocytes/macrophages[11–14] and DCs[10] in tissue healing early after

myocardial infarction. Nahrendorf, Swirski, and coworkers[12–14] have demonstrated that monocyte recruitment to the heart after acute infarction is dynamic and high and is dependent on extramedullary splenic hematopoiesis and mobilization of splenic monocytes (with accompanying loss of the splenic monocyte reservoir). This recruitment followed 2 phases—an initial infiltration of proinflammatory (Ly-6C^{hi}) monocytes (days 1–4 postinfarction) that promote tissue digestion, followed by reparative (Ly6C^{low}) monocytes that resolve inflammation and promote tissue healing. Wang et al[39] have shown an analogous proinflammatory state in the BM (increased CD11b^{+}, Gr-1^{+}, or Ly6C^{high} cells) early after infarction, which diminishes the reparative efficacy of BM-derived progenitors. This impaired efficacy resolved after the first week, consistent with an acute, time-limited process.

Extending these previous studies, our data reveal that chronic ischemic HF is characterized by Gr-1^{hi} monocytes in the blood and CD206^{-} macrophages in the failing heart well after the formation of healed infarct scar. Hence, infiltrating monocytes/macrophages in the chronically failing heart re-establish a proinflammatory and injurious phenotype[7,8,21] that promotes ongoing remote (and border) zone tissue remodeling. Importantly, the splenic proinflammatory monocyte reservoir remains depleted in chronic HF, especially in the SRP, similar to that observed early after infarction.[14] Unlike in the spleen, and contrary to the early postinfarct period,[39] we observed no changes in the activated monocyte population in the BM in HF. Therefore, our results suggest that in chronic HF there is persistent splenic mobilization of proinflammatory monocytes to the heart resulting in tissue infiltration by M1 macrophages that promote ongoing tissue remodeling. Persistently elevated serum levels of MCP-1 (C-C chemokine receptor type 2), a C-C chemokine that plays a critical role in the trafficking and tissue recruitment of proinflammatory monocytes after myocardial infarction,[7,11,40] provide further support for this scenario. These data are also consistent with human studies demonstrating increased numbers of activated monocytes in the circulation of patients with advanced HF.[41]

DCs are specialized for the processing and presentation of antigens to T-cells on upregulation of MHC and costimulatory molecules (eg, CD86). Depending on the DC functional subset, activation state, and maturation stage,[42] a variety of immune responses can be engendered, including helper or cytotoxic T-cell activation as well as T-cell immune tolerance.[6,22,26,33,43] DCs infiltrate into the heart early after infarction, peaking at 7 days, and are

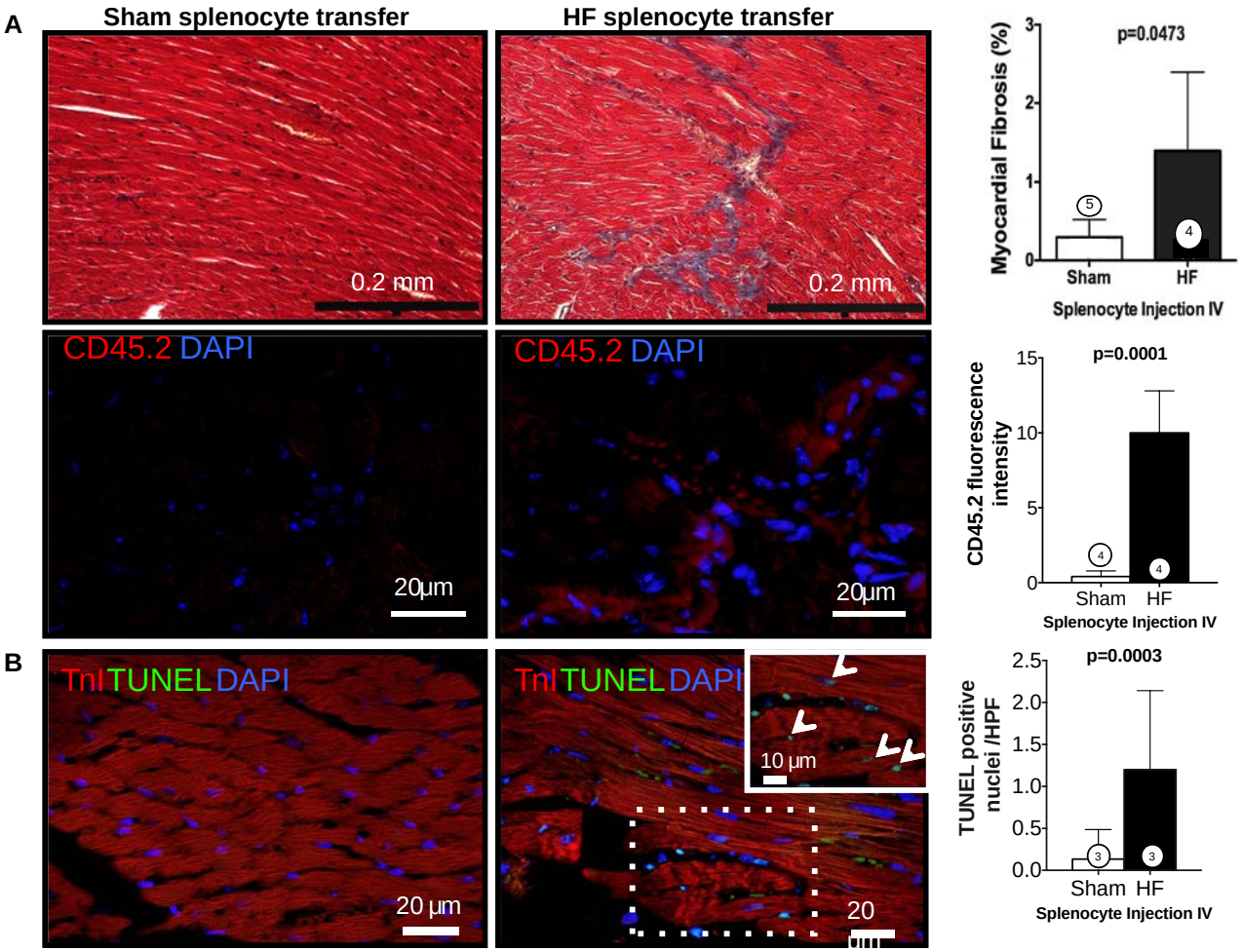

Figure 8. Continued

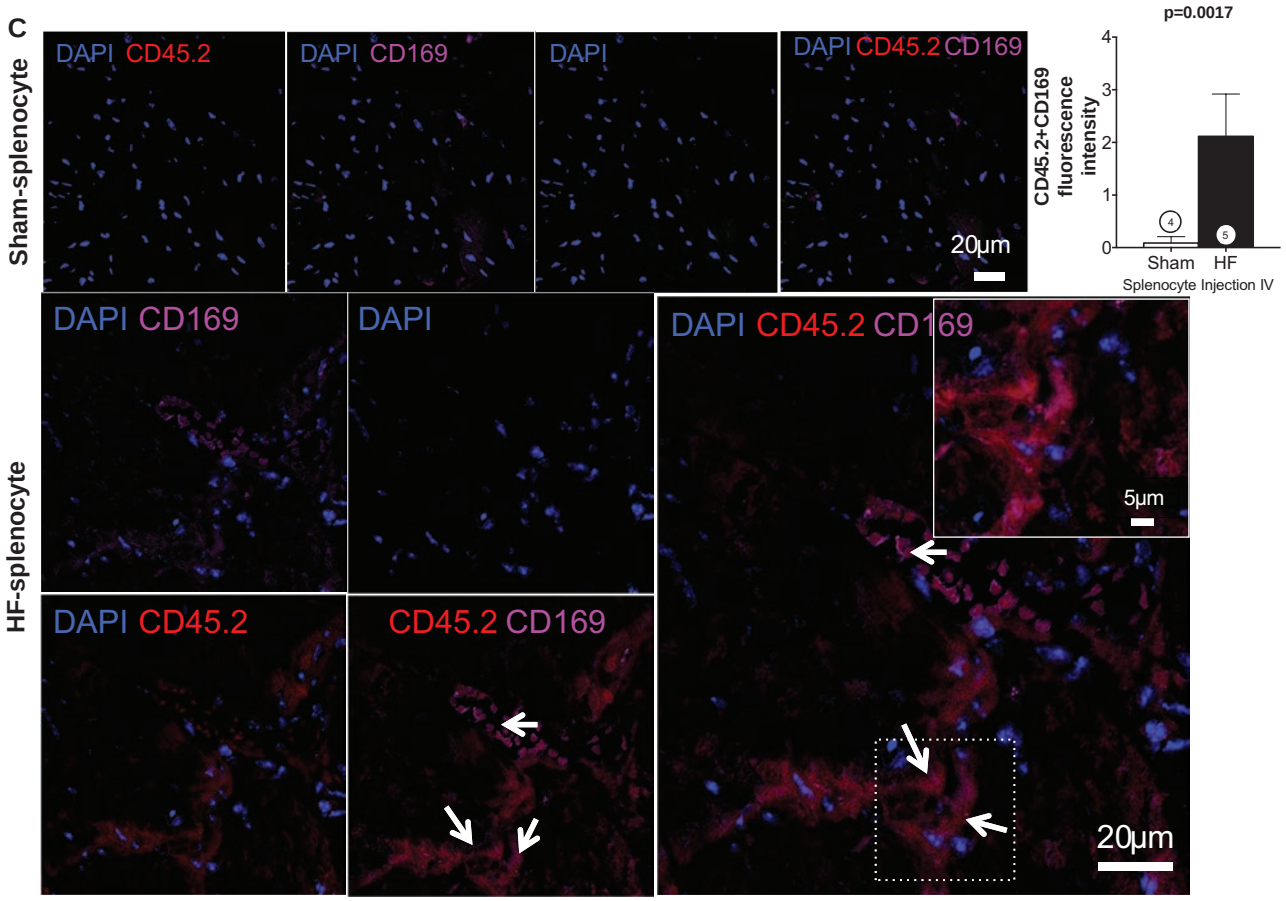

Figure 8. Trichrome and CD45.2 immunostains (A) and TUNEL stains (B) of hearts from heart failure (HF) or sham splenocyte recipient mice with corresponding quantification of myocardial fibrosis and apoptosis. CD45.2⁺ donor cells were frequently observed in interstitial and perivascular regions in HF splenocyte recipient hearts (**A**). **C**, Representative confocal images of CD45.2- and CD169-immunostained sections from sham and HF splenocyte recipient hearts and corresponding group data for CD45.2⁺CD169⁺ cells (arrows). N=3 to 5 per group (**A–C**).

immunoprotective, because selective DC ablation immediately after infarction worsened remodeling, enhanced inflammatory cytokines, and increased cardiac infiltration of proinflammatory monocytes.[10] Our results demonstrate that in chronic HF, well after the infarct healing period, there is a marked increase in cDC and pDC populations in the spleen and in the failing heart itself, together with increased circulating cDCs and augmented BM pDCs. Moreover, contrary to early postinfarction, this increase in DCs is accompanied by the mobilization and infiltration of proinflammatory monocytes and macrophages to the failing heart, suggesting a chronic and inappropriately activated deleterious immune response. Notably, although cDCs are potent activators of both CD8 and CD4 T-cells that can promote tissue damage,[6] mature pDCs are poorly immunostimulatory and favor the formation of regulatory T-cells and self-tolerance,[26,44] which can mitigate the same. In our study, the failing heart exhibited augmented levels of both immature and mature pDCs (Figure 2), presumably reflecting varying capacities for the induction of self-tolerance in response to tissue injury. Hence, the balance between cDCs and pDCs, as well as the relative abundance of maturing pDCs, may be of considerable importance in the maintenance, or alternatively resolution, of chronic inflammation in the failing heart.

Increased CD4⁺ and CD8⁺ T-cells in the spleen accompanied the augmented levels of DCs, suggesting ongoing processing and presentation of antigens by DCs to T-cells, thereby leading to T-cell activation and differentiation and subsequent generation of effector or memory immune responses.[45] Although the specific antigens responsible for triggering immune cell activation are not definitively answered by our study, we found marked upregulation of chemokine and TLR pattern recognition receptors, known to be differentially expressed on DCs[36] in HF splenocytes, and augmented extra- and intracellular levels of HMGB1 in HF spleens (Online Figures X–XI). These findings suggest that the ongoing release, collection, and processing of damage-associated molecular patterns, presumably derived from injured myocardium, contribute importantly to sustained activation of immune cells in chronic HF. Among the cDC subsets, CD8⁺ DCs are considered more robust stimulators of CD8⁺ cytotoxic T-lymphocytes[6,33] and Th-1 CD4⁺ helper T-cell responses[34]; they have, however, also been implicated in tolerance induction.[6,43] Dissecting the specific antigen- and cell-mediated determinants of immune activation

versus tolerance in HF would be critical for guiding potential therapeutic immunomodulation. In this regard, Eriksson et al[46] demonstrated that BM-derived DCs self-loaded with α-myosin heavy chain peptide and activated with LPS and a CD40 stimulatory antibody induced $CD4^+$ T-cell–mediated myocarditis and subsequent HF. We propose that chronic remodeling in HF after myocardial infarction is also driven, at least in part, by sustained DC activation in response to cardiac antigens. HF is generally considered a T helper cell pathway-1 activation state—this would necessarily implicate DCs, regulators of $CD4^+$ T helper cell polarization, as critical mediators of the inflammatory response.

Newly Uncovered Robust Cardiosplenic Axis in Chronic HF

Global alterations of the mononuclear phagocyte network suggest significant underlying changes in the spleen, because 2 important functions of the spleen are to filter blood and to remove or initiate immune responses to circulating antigens.[32] Our results demonstrate striking changes in splenic architecture (more follicles, large germinal centers, and prominent marginal zones) and cell populations (augmented $CD8^+/CD8^-$ cDCs and pDCc, shift in the spatial distribution of DCs to the white pulp germinal centers, augmented $CD4^+$ and $CD8^+$ T-cells) that signify amplified antigen processing in HF. Also, the spleen exhibited depletion of SRP monocytes, connoting a reduced ability of the spleen in HF to remove (by phagocytosis) senescent erythrocytes and circulating particulates.[32] Hence, profound splenic remodeling occurs in chronic HF, which supports immune system activation, on the one hand, and diminished circulating antigenic clearance, on the other.

To evaluate the importance of these splenic abnormalities in HF, we selected 2 approaches to establish both the necessity and the sufficiency of the spleen for pathological cardiac remodeling. To establish necessity, we performed splenectomy in mice with chronic HF and evaluated LV structure and function 8 weeks later. Splenectomy both stabilized and actually reversed cardiac remodeling, with long-term improvement in LV ejection fraction and reduction in chamber size and suppression of $CD11b^+$ and $CD11c^+$ cell infiltration in the failing heart. Importantly, splenectomy did not significantly diminish circulating proinflammatory cytokines, suggesting primary effects referable to the cardiac recruitment of splenic immune cell populations rather than global levels of inflammatory mediators. Hence, the spleen exacerbates disease progression and cardiac inflammation in chronic HF. These results are counter to the beneficial role of the spleen early after infarction. Splenectomy at the time of infarction or 3 days later worsened scar formation and subsequent LV remodeling,[12] an effect thought to be because of wound healing responses engendered by the splenic monocyte reservoir. In contrast to this early effect, our data establish that in chronic HF, the spleen, with sustained depletion of SRP monocytes and increased antigenic processing, assumes a much more proinflammatory role and promotes mobilization of immune cell populations to the heart, which exacerbate detrimental LV remodeling.

To establish sufficiency of the spleen, we performed adoptive transfer of mononuclear splenocytes into otherwise normal naive mice. Importantly, our study design did not include additional exogenous mitogenic stimulation of splenocytes as has been reported previously in a study in rats.[47] Transfer of splenocytes from mice with HF, but not from sham-operated mice, recapitulated multiple facets of chronic pathological remodeling in naive mice. Notably, there were no discernible early effects on LV function, indicating a low likelihood of an acute myocarditis after transfer. Although donor splenocytes disappeared from the recipient mouse circulation <2 weeks, pathological changes were manifested in recipient hearts much later, at 8 weeks, and included LV dilatation, hypertrophy (by gravimetric analysis), systolic dysfunction, and myocardial apoptosis and fibrosis. Moreover, we found evidence of donor splenocytes homing to recipient hearts, localized primarily at sites of interstitial fibrosis and in perivascular regions. Intriguingly, systemic changes were also evident, including splenic hypertrophy with architectural changes similar to those seen in HF and increased levels of circulating activated monocytes consistent with an inflammatory state.

This effect was specific to splenocytes from HF, because there were no substantial changes in systemic cytokine levels and because adoptive transfer of splenocytes from mice treated with LPS had no discernible cardiac effects. Moreover, the high level of expression of cytokine/chemokine mediators, TLRs, and alarmins in HF splenocytes indicates that these cells were potently activated and suggested that the recapitulation of systemic inflammation and tissue injury/remodeling in naive hearts occurred as a result of previous priming of splenic immune cells to cardiac antigens in HF. Hence, taken together, our results suggest that the spleen is a fundamental mediator of chronic inflammation and remodeling in HF; activated splenocytes (potentially in response to cardiac alarmins) home to the heart to induce tissue injury; and HF splenocytes retain memory sufficient for recreating the injurious immune responses in otherwise normal animals. These data suggest that remodeling progression in chronic HF is an immune cell–mediated phenomenon and that targeting specific mononuclear cell populations within the spleen and heart (eg, monocyte/macrophages and DCs), or the specific antigens responsible for their activation, may comprise a more feasible approach to therapeutic immunomodulation in this disease. The relative importance of each specific cell type in this disease process and the identity and importance of specific antigens and alarmins will require further study.

In summary, we have demonstrated profound remodeling of the mononuclear phagocyte network and the spleen in HF, which forms the basis for chronic inflammation. These changes, which are consistent with ongoing, enhanced antigen processing in the spleen and sustained inflammatory/immune cell–mediated injury in the failing heart, are of pathophysiological importance for the progression of HF, independent of other factors. Hence, we propose the novel paradigm that mononuclear phagocytes are obligatory disease mediators in HF and that progression of pathological cardiac remodeling is dependent, at least in part, on autoimmune injury in the heart induced by these cell populations.

Acknowledgments

We gratefully acknowledge James F. George, PhD, and his laboratory for their assistance in performing the splenocyte adoptive transfer studies.

Sources of Funding

This work was supported by a VA Merit Award (to S.D.P.), National Institutes of Health grants HL-78825 and HL-99014 (to S.D.P.), and an American Heart Association SDG award 0835456 N (to T.H.).

Disclosures

None.

References

1. Mann DL. Inflammatory mediators and the failing heart: past, present, and the foreseeable future. *Circ Res*. 2002;91:988–998.
2. Bozkurt B, Mann DL, Deswal A. Biomarkers of inflammation in heart failure. *Heart Fail Rev*. 2010;15:331–341.
3. Hamid T, Gu Y, Ortines RV, Bhattacharya C, Wang G, Xuan YT, Prabhu SD. Divergent tumor necrosis factor receptor-related remodeling responses in heart failure: role of nuclear factor-kappaB and inflammatory activation. *Circulation*. 2009;119:1386–1397.
4. Braunwald E. Biomarkers in heart failure. *N Engl J Med*. 2008;358:2148–2159.
5. Prabhu SD. Cytokine-induced modulation of cardiac function. *Circ Res*. 2004;95:1140–1153.
6. Kushwah R, Hu J. Complexity of dendritic cell subsets and their function in the host immune system. *Immunology*. 2011;133:409–419.
7. Ingersoll MA, Platt AM, Potteaux S, Randolph GJ. Monocyte trafficking in acute and chronic inflammation. *Trends Immunol*. 2011;32:470–477.
8. Biswas SK, Mantovani A. Macrophage plasticity and interaction with lymphocyte subsets: cancer as a paradigm. *Nat Immunol*. 2010;11: 889–896.
9. Geissmann F, Manz MG, Jung S, Sieweke MH, Merad M, Ley K. Development of monocytes, macrophages, and dendritic cells. *Science*. 2010;327: 656–661.
10. Anzai A, Anzai T, Nagai S, et al. Regulatory role of dendritic cells in postinfarction healing and left ventricular remodeling. *Circulation*. 2012;125:1234–1245.
11. Frangogiannis NG. Regulation of the inflammatory response in cardiac repair. *Circ Res*. 2012;110:159–173.
12. Leuschner F, Rauch PJ, Ueno T, et al. Rapid monocyte kinetics in acute myocardial infarction are sustained by extramedullary monocytopoiesis. *J Exp Med*. 2012;209:123–137.
13. Nahrendorf M, Pittet MJ, Swirski FK. Monocytes: protagonists of infarct inflammation and repair after myocardial infarction. *Circulation*. 2010;121:2437–2445.
14. Swirski FK, Nahrendorf M, Etzrodt M, Wildgruber M, Cortez-Retamozo V, Panizzi P, Figueiredo JL, Kohler RH, Chudnovskiy A, Waterman P, Aikawa E, Mempel TR, Libby P, Weissleder R, Pittet MJ. Identification of splenic reservoir monocytes and their deployment to inflammatory sites. *Science*. 2009;325:612–616.
15. Wang G, Hamid T, Keith RJ, et al. Cardioprotective and antiapoptotic effects of heme oxygenase-1 in the failing heart. *Circulation*. 2010;121:1912–1925.
16. Hamid T, Guo SZ, Kingery JR, Xiang X, Dawn B, Prabhu SD. Cardiomyocyte NF-κB p65 promotes adverse remodelling, apoptosis, and endoplasmic reticulum stress in heart failure. *Cardiovasc Res*. 2011;89:129–138.
17. Lavelle GC, Sturman L, Hadlow WJ. Isolation from mouse spleen of cell populations with high specific infectivity for scrapie virus. *Infect Immun*. 1972;5:319–323.
18. Austyn JM, Hankins DF, Larsen CP, Morris PJ, Rao AS, Roake JA. Isolation and characterization of dendritic cells from mouse heart and kidney. *J Immunol*. 1994;152:2401–2410.
19. Fleming TJ, Fleming ML, Malek TR. Selective expression of Ly-6G on myeloid lineage cells in mouse bone marrow. RB6-8C5 mAb to granulocyte-differentiation antigen (Gr-1) detects members of the Ly-6 family. *J Immunol*. 1993;151:2399–2408.
20. Robbins CS, Swirski FK. The multiple roles of monocyte subsets in steady state and inflammation. *Cell Mol Life Sci*. 2010;67:2685–2693.
21. Gordon S, Taylor PR. Monocyte and macrophage heterogeneity. *Nat Rev Immunol*. 2005;5:953–964.
22. Shortman K, Naik SH. Steady-state and inflammatory dendritic-cell development. *Nat Rev Immunol*. 2007;7:19–30.
23. Hadeiba H, Lahl K, Edalati A, Oderup C, Habtezion A, Pachynski R, Nguyen L, Ghodsi A, Adler S, Butcher EC. Plasmacytoid dendritic cells transport peripheral antigens to the thymus to promote central tolerance. *Immunity*. 2012;36:438–450.
24. Hochrein H, O'Keeffe M, Wagner H. Human and mouse plasmacytoid dendritic cells. *Hum Immunol*. 2002;63:1103–1110.
25. Blasius AL, Colonna M. Sampling and signaling in plasmacytoid dendritic cells: the potential roles of Siglec-H. *Trends Immunol*. 2006;27:255–260.
26. Ito T, Yang M, Wang YH, Lande R, Gregorio J, Perng OA, Qin XF, Liu YJ, Gilliet M. Plasmacytoid dendritic cells prime IL-10-producing T regulatory cells by inducible costimulator ligand. *J Exp Med*. 2007;204:105–115.
27. Kitchen SG, Jones NR, LaForge S, Whitmire JK, Vu BA, Galic Z, Brooks DG, Brown SJ, Kitchen CM, Zack JA. CD4 on CD8(+) T cells directly enhances effector function and is a target for HIV infection. *Proc Natl Acad Sci U S A*. 2004;101:8727–8732.
28. Ismahil MA, Hamid T, Haberzettl P, Gu Y, Chandrasekar B, Srivastava S, Bhatnagar A, Prabhu SD. Chronic oral exposure to the aldehyde pollutant acrolein induces dilated cardiomyopathy. *Am J Physiol Heart Circ Physiol*. 2011;301:H2050–H2060.
29. Wang HX, Yi SQ, Li J, Terayama H, Naito M, Hirai S, Qu N, Yi N, Itoh M. Effects of splenectomy on spontaneously chronic pancreatitis in aly/aly mice. *Clin Dev Immunol*. 2010;2010:614890.
30. Kodama M, Matsumoto Y, Fujiwara M. In vivo lymphocyte-mediated myocardial injuries demonstrated by adoptive transfer of experimental autoimmune myocarditis. *Circulation*. 1992;85:1918–1926.
31. Pinto AR, Paolicelli R, Salimova E, Gospocic J, Slonimsky E, Bilbao-Cortes D, Godwin JW, Rosenthal NA. An abundant tissue macrophage population in the adult murine heart with a distinct alternatively-activated macrophage profile. *PLoS One*. 2012;7:e36814.
32. Cesta MF. Normal structure, function, and histology of the spleen. *Toxicol Pathol*. 2006;34:455–465.
33. Joffre OP, Segura E, Savina A, Amigorena S. Cross-presentation by dendritic cells. *Nat Rev Immunol*. 2012;12:557–569.
34. Maldonado-López R, De Smedt T, Michel P, Godfroid J, Pajak B, Heirman C, Thielemans K, Leo O, Urbain J, Moser M. CD8alpha+ and CD8alpha- subclasses of dendritic cells direct the development of distinct T helper cells in vivo. *J Exp Med*. 1999;189:587–592.
35. den Haan JM, Kraal G. Innate immune functions of macrophage subpopulations in the spleen. *J Innate Immun*. 2012;4:437–445.
36. Kaisho T. Pathogen sensors and chemokine receptors in dendritic cell subsets. *Vaccine*. 2012;30:7652–7657.
37. Chan JK, Roth J, Oppenheim JJ, Tracey KJ, Vogl T, Feldmann M, Horwood N, Nanchahal J. Alarmins: awaiting a clinical response. *J Clin Invest*. 2012;122:2711–2719.
38. Timmers L, Pasterkamp G, de Hoog VC, Arslan F, Appelman Y, de Kleijn DP. The innate immune response in reperfused myocardium. *Cardiovasc Res*. 2012;94:276–283.
39. Wang X, Takagawa J, Lam VC, Haddad DJ, Tobler DL, Mok PY, Zhang Y, Clifford BT, Pinnamaneni K, Saini SA, Su R, Bartel MJ, Sievers RE, Carbone L, Kogan S, Yeghiazarians Y, Hermiston M, Springer ML. Donor myocardial infarction impairs the therapeutic potential of bone marrow cells by an interleukin-1-mediated inflammatory response. *Sci Transl Med*. 2011;3:100ra90.
40. Dewald O, Zymek P, Winkelmann K, Koerting A, Ren G, Abou-Khamis T, Michael LH, Rollins BJ, Entman ML, Frangogiannis NG. CCL2/Monocyte Chemoattractant Protein-1 regulates inflammatory responses critical to healing myocardial infarcts. *Circ Res*. 2005;96:881–889.
41. Conraads VM, Bosmans JM, Schuerwegh AJ, Goovaerts I, De Clerck LS, Stevens WJ, Bridts CH, Vrints CJ. Intracellular monocyte cytokine production and CD 14 expression are up-regulated in severe vs mild chronic heart failure. *J Heart Lung Transplant*. 2005;24:854–859.
42. Mahnke K, Schmitt E, Bonifaz L, Enk AH, Jonuleit H. Immature, but not inactive: the tolerogenic function of immature dendritic cells. *Immunol Cell Biol*. 2002;80:477–483.
43. Shortman K, Heath WR. The CD8+ dendritic cell subset. *Immunol Rev*. 2010;234:18–31.
44. Matta BM, Castellaneta A, Thomson AW. Tolerogenic plasmacytoid DC. *Eur J Immunol*. 2010;40:2667–2676.
45. Brownlie RJ, Zamoyska R. T cell receptor signalling networks: branched, diversified and bounded. *Nat Rev Immunol*. 2013;13:257–269.

46. Eriksson U, Ricci R, Hunziker L, Kurrer MO, Oudit GY, Watts TH, Sonderegger I, Bachmaier K, Kopf M, Penninger JM. Dendritic cell-induced autoimmune heart failure requires cooperation between adaptive and innate immunity. *Nat Med*. 2003;9:1484–1490.

47. Maisel A, Cesario D, Baird S, Rehman J, Haghighi P, Carter S. Experimental autoimmune myocarditis produced by adoptive transfer of splenocytes after myocardial infarction. *Circ Res*. 1998;82:458–463.

Novelty and Significance

What Is Known?

- Sustained local and systemic inflammatory activation are hallmarks of chronic heart failure (HF).
- Inflammatory cells such as mononuclear phagocytes, that is, monocytes/macrophages and dendritic cells (DCs), are both important sources and effector targets for proinflammatory cytokines.
- Although monocytes/macrophages and DCs are known to contribute importantly to cardiac remodeling early after myocardial infarction, their role in chronic HF is unknown.

What New Information Does This Article Contribute?

- Anomalies of the global mononuclear phagocyte network underlie the persistent inflammation in chronic HF and promote the cardiac residence of proinflammatory monocytes/macrophages, classical DCs (cDCs), and plasmacytoid DCs (pDCs).
- In HF, the spleen exhibits heightened antigen processing together with reductions in the splenic monocyte reservoir, but augmentation of cDCs and pDCs and increased expression of alarmins and proinflammatory mediators.
- The cardiosplenic axis plays an obligatory role in the pathogenesis and progression of cardiac remodeling in HF, because splenectomy reversed left ventricular (LV) remodeling and inflammation, whereas adoptive transfer of HF-derived mononuclear splenocytes into naive mice reproduced long-term cardiac remodeling.

Whether inflammatory cells can be manipulated for therapeutic benefit in HF is unknown. In this study, we show profound alterations in the mononuclear phagocyte network in HF, which include increased proinflammatory macrophages and monocytes in the failing heart and circulation, and augmented cDCs and pDCs in the heart and spleen. We also demonstrate marked splenic remodeling in HF, indicative of heightened antigen processing, in concert with robust splenocyte expression of alarmins and proinflammatory mediators and augmented splenic $CD4^+$ and $CD8^+$ T-cells. Finally, we show that the spleen is indispensable for remodeling progression and inflammation in HF, because splenectomy reversed remodeling and attenuated cardiac macrophage and DC infiltration, and mononuclear splenocytes from HF mice homed to the heart and induced long-term cardiac remodeling, apoptosis, fibrosis, dysfunction, and systemic inflammation on adoptive transfer into naive mice. Hence, we propose the novel paradigm that adverse LV remodeling in chronic ischemic HF is in part immune cell–mediated, potentially in response to cardiac-derived alarmins, and that targeting specific monocyte/macrophage and DC populations within the spleen and heart, or the antigens responsible for their activation, may comprise a more feasible approach to therapeutic immunomodulation in this disease.

EXPANDED METHODS

All studies were performed in compliance with the NIH Guide for the Care and Use of Laboratory Animals (DHHS publication No. [NIH] 85-23, revised 1996). The University of Alabama at Birmingham Institutional Animal Care and Use Committee gave local approval for these studies. The total of 120 mice were used.

Mouse models and surgical protocol. Male C57BL/6J mice 10-12 weeks of age (Jackson Laboratories, stock #000664) were used. To induce pathological LV remodeling and HF, the mice underwent left thoracotomy and left coronary artery ligation (n=19) as previously described.[1-3] Sham operated mice (n=12) were used as controls. Anesthesia was induced in mice with tribromoethanol (0.25 mg/g IP). Mice were then intubated and ventilated with a MiniVent Mouse Ventilator (Type 845, Harvard Apparatus) at 125-150 breaths/minute, with anesthesia maintained using 1-2% isoflurane and body temperature kept at 37°C using heat lamps and heating pads. Using sterile technique, mice were subjected to a thoracotomy in the 4th intercostal space. With the aid of a dissecting microscope, the proximal left coronary artery was visualized and permanently occluded with 8.0-prolene suture, 1 mm distal to the left atrial appendage border. Successful occlusion was confirmed by the production of pallor and dyskinesia in the distal myocardium. In sham animals, the suture was passed but not tied. The chest was then closed in layers using 5.0 silk and the mice were weaned off isoflurane anesthesia. Upon recovery of spontaneous respiration, the intubation tube was removed and the mice were recovered in a temperature-controlled area supplemented with 100% oxygen. The mice were then followed for 8 weeks after operation and evaluated for the various readouts.

Echocardiography. Mouse echocardiography was performed under anesthesia with tribromoethanol (0.25 mg/g IP), and light (~1%) isoflurane as needed, using a VisualSonics Vevo 770 High-Resolution System with a RMV707B scanhead. Mice were imaged on a heated, bench-mounted adjustable rail system (Vevo Imaging Station) that allowed steerable and hands-free manipulation of the ultrasound transducer. Two echocardiographers performed the

studies and were blinded as to the specific experimental group. Left ventricular (LV) end-diastolic and end-systolic volumes (EDV and ESV) were planimetered from the long-axis images using the modified Simpson's method. LV systolic function was indexed by single plane LV ejection fraction (EF = [EDV-ESV]/EDV).

Isolation of splenocytes. Eight weeks after coronary ligation or sham operation, the spleen was removed aseptically and placed in a 35 mm tissue culture dish with ~5 mL of DMEM culture medium (Gibco, Invitrogen). Splenocytes were isolated according to the protocol of Lavelle at al,[4] with slight modifications. Briefly, the spleen was finely minced using a scalpel. Repeated pipetting was used to disperse cells from minced fragments, and single cells were transferred to a fresh tube and kept on ice. For larger tissue pieces, the procedure was repeated several times in the dish with fresh DMEM. The final cell suspension was pipetted through a nylon cell strainer, 100 μm (BD Falcon), into a fresh tube and centrifuged at 150*g* for 5 min at 4°C. The supernatant was decanted, and the pellet re-suspended in 0.4 ml of RBC lysis buffer (eBiosciences) for 5 min at room temperature (RT). The addition of fresh DMEM neutralized the erythrocyte lysis. Pelleted splenocytes were then re-suspended in fresh DMEM (0.5-1.0 mL).

Isolation of bone marrow (BM) and peripheral blood cells. After mice were sacrificed, femurs and tibiae were dissected from the adherent soft tissue. The tip of each bone was removed with scissors, and the marrow was flushed with DMEM using a 27-gauge needle and aspirated. BM cells were filtered through a 100 μm nylon cell strainer (BD Falcon), sedimented at 150*g* for 5 min at 4°C, and re-suspended in RBC lysis buffer. After complete erythrocyte lysis, BM cells were re-suspended in fresh 1-2 mL DMEM.

Peripheral blood (~500 μL) was collected in BD Microtainer tubes with EDTA. Erythrocytes were lysed with 2 mL RBC lysis buffer for 5 min on ice. Leukocytes were collected by centrifugation (380*g* for 10 min at 4°C), and resuspended in 400 uL of ice-cold flow cytometry staining buffer (eBioscience).

Isolation of mononuclear cells from the heart. Single mononuclear cells were isolated from sham and failing hearts following the method of Austyn et al.[5] Mouse hearts were excised *in toto* and placed in heparinized saline. After removal of epicardial fatty tissue and the aorta, the heart was finely minced into ~1-2 mm pieces and blood was removed by repeated washing in saline (with stepwise reductions in added heparin). The tissue was digested with collagenase (Worthington, 1mg/ml), trypsin (Gibco, Invitrogen, 0.1%), and DNAse (5 Prime, 10 µg/ml) in 10 mL RPMI media (Gibco) for 45 min at 37°C with occasional shaking. Released cells were separated from solid tissue by filtering through a 100 µm nylon cell strainer (BD Falcon), washed with R10 media (RPMI-1640 supplemented with 10% heat-inactivated FCS, 2mM-L-Glutamine, 25 µM-2-Mercaptoethanol, 1% penicillin/streptomycin), and placed on ice. These steps were repeated 2-3 times to digest the remaining tissue. Any residual solid tissue was treated sequentially with EDTA (2 mM) in digestion media for 10 min at 37^{o}C, collagenase (2 mg/ml) in R10 media for 20 min at 37^{o}C, and released cells filtered through the strainer. All collected cells were pooled and pelleted at 150*g* for 5 min at 4^{o}C. Single cell suspensions were layered on Ficoll gradient solution and centrifuged at 2000*g* for 20 min. To reduce myocyte contamination in the mononuclear cell suspension, 75% of the total volume (excepting cell debris) was collected and washed in R10 media. The presence of nucleated cells was confirmed by DAPI staining during flow cytometry analysis. In a separate aliquot, cell viability (>80%) was confirmed using the trypan blue exclusion method.

Flow Cytometry. Isolated cell suspensions were incubated for 30 min at RT in a cocktail of fluorophore-labeled mAbs (BD Biosciences or as otherwise indicated), as appropriate for the specific study, against: F4/80-Pacific Blue; CD8-FITC; CD45R/B220-APC; CD11b-605-NC (eBiosciences); Gr-1-APC (eBiosciences); CD11c-PE-Cy7; CD86-PE-Cy5; CD206-FITC; Siglec-H-efluor 660 (eBiosciences), CD45.1-FITC (Miltenyi Biotech); CD45.2-PE. Lineage (Lin)1 antibody cocktail was used for DC identification (to exclude thymocytes: CD90.2-PE, natural killer cells: NK1.1-PE, CD49B-PE, and granulocytes: Gr-1-PE), and Lin2 antibody cocktail was

used for macrophage/monocyte subset identification (CD90.2-PE, NK1.1-PE, CD49B-PE, and CD45R/B220-PE for B-cells). In separate assessments of splenic T-cells, cell suspensions were incubated with CD3-FITC, CD4-650 NC and CD8-605 NC (eBiosciences). Of note, the anti-Gr-1 antibody recognizes both Ly6C and Ly6G antigens.[6]

Activated macrophages/monocytes were identified as $CD11b^{+}F4/80^{+}$ cells.[7, 8] Pro-inflammatory monocytes were identified as $Lin2^{-}CD11b^{+}F4/80^{+}Gr\text{-}1^{hi}$ and anti-inflammatory monocytes as $Lin2^{-}CD11b^{+}F4/80^{+}Gr\text{-}1^{low}$ cells.[7-10] Pro-inflammatory M1 and anti-inflammatory M2 macrophages in tissue were sub-classified from $Lin2^{-}CD11b^{+}F4/80^{+}$ cells based on the absence or presence of CD206 (mannose receptor) expression.[11] Dendritic cells were identified as $Lin1^{-}CD11c^{+}$ cells.[9, 10, 12] Classical dendritic cells (cDC) were identified as $Lin1^{-}CD11c^{+}B220^{-}$, whereas non-classical plasmacytoid dendritic cells (pDC) were identified as $Lin1^{-}CD11c^{+/low}B220^{+}$.[10, 12-14] In some studies, pDCs were identified as Siglec-H^{+} cells.[15] Lymphoid cDCs were further subdivided as $CD8^{+}$ or $CD8^{-}$,[10, 12] and pDCs as $CD86^{+}$ or $CD86^{-}$ (classical costimulatory molecule and marker of pDC maturity).[16] Helper and cytotoxic T-cells were characterized as $CD3^{+}CD4^{+}$ and $CD3^{+}CD8^{+}CD4^{-}$ cells, respectively.[17] For the heart, spleen, and BM, identified cells were normalized for total cell population. For peripheral blood, cell numbers were normalized for the total lymphocyte and monocyte gate. Data were acquired on an LSRII flow cytometer (BD Biosciences) and analyzed with FlowJo software, version 7.6.3.

Immunohistochemistry and confocal microscopy. Formalin-fixed, paraffin-embedded hearts and spleens from sham and HF mice were sectioned at 5 μm thickness, deparaffinized and rehydrated; (immuno)histological staining was performed as previously described.[1, 3] Masson's trichrome was used to evaluate tissue fibrosis and general histology (heart and spleen), and Alexa Fluor 488-conjugated wheat-germ agglutinin (WGA; Invitrogen) for myocyte area.

Myocardial apoptosis was evaluated using the DeadEnd Fluorometric TUNEL System (Promega) as previously described.[3, 18] This assay kit catalytically incorporates fluorescein-12-

dUTP at the 3′-ends of fragmented DNA in apoptotic cells using recombinant terminal deoxynucleotidyl transferase (rTdT). Deparaffinized and rehydrated tissue sections were treated with Proteinase K (20 µg/ml) for 15 min at 37°C and then fixed with 4% methanol-free formaldehyde solution in PBS. All subsequent steps were performed following the manufacturer's instructions. Cardiomyocytes were identified by staining with anti-troponin I antibody (Santa Cruz Biotechnology) followed by Alexa Fluor 555-conjugated secondary antibody (Invitrogen) using the protocol below, and sections were counterstained with 4’,6-diamidino-2-phenylindole (DAPI, Invitrogen) to label nuclei blue. TUNEL-positive nuclei (cyan staining) were visualized directly by confocal microscopy (Zeiss LSM710) with nuclear staining confirmed using *z*-axis sections. Images were taken with a 63x objective lens at five different locations in each tissue section. DNase (10 U/ml)-treated sections were used as positive controls. Sections without rTdT treatment were used as negative controls.

For immunostaining, deparaffinized and rehydrated sections were incubated for 20 min with 10 mmol/L citric acid (pH 6.0) and then treated with enzymatic antigen retrieval to recover antigenicity. Nonspecific binding was blocked with 5% normal goat serum and 0.05% saponin (Sigma) in PBS (pH 7.4) for 30 min. Sections were blocked and then incubated with the appropriate primary antibody in PBS with 1% BSA and 0.05% saponin for 1 h at 37°C against: CD11b/ITAM (Epitomics), CD11c (eBiosciences), F4/80 (eBiosciences), CD169 (R&D Systems), high mobility group box-1 (HMGB1, IBL International), and CD45.2-PE (BD Biosciences). Tissue sections were then incubated for 30 min at room temperature with respective secondary secondary antibodies conjugated with Alexa 488, 555, or 647 (Invitrogen), and counterstained with DAPI to label nuclei. Images were made with a 63x objective lens at five different locations in each tissue section. Mean fluorescence intensity was evaluated using imageJ 1.47V software for at least five images/heart.

Myocyte area and cardiac fibrosis were quantified from 5-6 high-power fields per section in the remote non-infarcted area of the heart using Image J and Metamorph software,

respectively. In the spleen, CD11b positive cells in the subcapsular red pulp were counted in 3-5 high power fields per section. Data for each group were calculated from 12-15 sections and 4-5 mice from each group. The measurements and calculations were conducted in a blinded manner. Confocal microscopy was carried out on an LSM710 microscope (Zeiss) and Z-stack images were acquired according to standard protocols.

Cytometric bead array (CBA) immunoassay for serum cytokines. Peripheral blood was allowed to clot at RT for 2 h. After centrifugation at 2,000 rpm for 10 min, serum was collected and stored at −20°C until assays were performed. Serum concentrations of TNF, monocyte chemoattractant protein (MCP)-1, interferon (IFN)-γ, interleukin (IL)-6, IL-10, and IL-12p70 were measured simultaneously using a CBA Mouse Inflammation Kit (BD Biosciences). Briefly, 50 µL of chemokine capture bead mixture was incubated with 50 µL of either recombinant standard or sample and 50 µL of PE-conjugated detection antibody for 2 h at RT. The mixture was washed to remove unbound PE detection reagent before data acquisition on a BD LSRII flow cytometer. Analysis was performed using FCAP Array software.

Splenocyte gene expression by quantitative real-time PCR. Mononuclear splenocytes were cultured in serum free DMEM media for 24 h after isolation (2-3 X 10^6 cells/well). The cells were then collected and stored at -80^0C in TRIzol reagent (Invitrogen) for subsequent RNA isolation. Total RNA levels were quantified and sample purity assessed using the ratio of absorbance at 260 and 280 nm by NanoDrop 1000 Spectrophotometer (Thermo Scientific). Subsequent cDNA synthesis and quantitative real-time PCR using SYBR Green (Life Technologies) were performed as described previously.[1, 2, 18] Briefly, total RNA (500 ng) was reversed transcribed using High Efficiency cDNA Synthesis Kit (Life Technologies). Relative levels of mRNA transcripts for TNF, IL-1β, IL-2, IL-4, IL-5, IL-6, IL-10, IL-13, IFN-γ, inducible nitric oxide synthase (iNOS), C-C chemokine receptor type 2 (CCR2), CCR5, chemokine (C-C motif) ligand 5 (CCL5), chemokine (C-X-C motif) receptor 3 (CXCR3), CX3C chemokine receptor 1 (CX3CR1), toll-like receptor (TLR)1, TLR7, TLR9, TLR12, transforming growth factor

(TGF)-β, HMGB1, S100A8, S100A9, and galectin-3 were determined using forward and reverse primer pairs detailed in Supplemental Table I, and normalized to 18s rRNA expression using the $\Delta\Delta C_T$ comparative method.[1]

Survival splenectomy and splenocyte adoptive transfer. In a separate sub-group, male (CD 45.2) C57BL/6J mice (n = 36) underwent coronary ligation or sham operation. Eight weeks later, survival splenectomy (or, in some mice, sham abdominal surgery) was performed using standard surgical techniques.[19] Briefly, mice were anesthetized with tribromoethanol (0.25 mg/g IP) and anesthesia was maintained with 1% isoflurane as needed. After sterilizing the surgical area, a ~1 cm incision was made in the left subcostal region, and the peritoneum was opened to exteriorize the spleen. The spleen was retracted away from the pancreatic tail, the splenic bundle was ligated at the hilum using 8.0 prolene ligature, and then the spleen was removed intact. For sham operations, the splenic bundle and spleen were left intact. The procedure required ~10–15 minutes to complete; totality of splenectomy was ensured by close examination at the time of operation and confirmed during postmortem examination. Splenocytes from sham-operated and HF mice were used for the adoptive transfer studies described below. Splenectomized mice (and sham abdominal surgery controls) were subsequently followed for 8 more weeks with serial echocardiography.

For adoptive transfer studies, splenocytes were prepared as described previously.[20] Briefly, single cell suspensions were prepared from spleens isolated from sham-operated (n=8) and HF mice (n=7). The erythrocytes were lysed with RBC lysis buffer (eBioscience, CA). Single cell suspensions were then layered on Ficoll-Paque (GE Healthcare) gradient and centrifuged at 2000*g* for 20 min to separate mononuclear cells and exclude granulocytes and residual erythrocytes. Mononuclear cells were collected, washed three times with sterile PBS, and resuspended in sterile PBS. Cells were then pooled from either sham or HF mice and resuspended in 5 ml PBS. Mononuclear cells were injected (~17 X 10^6 cells in 100 µL PBS per animal via tail vein) into naïve CD 45.1 C57BL/6J mice (7 mice receiving sham splenocytes and

7 mice receiving HF splenocytes).

As an additional control for adoptive transfer, we also isolated splenocytes from CD45.2 C57BL/6J mice (male, 6-8 weeks) treated with either lipopolysaccharide (LPS) to induce systemic inflammation or PBS control. LPS (0.4 mg/kg) or PBS (0.2 mL) was injected i.p. daily for two consecutive days (n = 5 per group). Spleens were aseptically harvested 24 h after the last i.p. dose, and the mononuclear cell population was isolated and injected via tail vein into naïve CD45.1 C57BL/6 recipient mice (n = 7 per group receiving either LPS-splenocytes or PBS-splenocytes) as above.

Statistical Analysis. Continuous data are summarized as mean ± standard deviation (SD). Statistical comparisons were performed using the unpaired student's t-test when comparing two groups. For comparisons of more than two groups, two-way ANOVA was used with Bonferroni post-test to adjust for multiple comparisons. A p value of < 0.05 was considered statistically significant.

REFERENCES

1. Hamid T, Gu Y, Ortines RV, Bhattacharya C, Wang G, Xuan YT, Prabhu SD. Divergent tumor necrosis factor receptor-related remodeling responses in heart failure: Role of nuclear factor-κB and inflammatory activation. *Circulation*. 2009;119:1386-1397
2. Hamid T, Guo SZ, Kingery JR, Xiang X, Dawn B, Prabhu SD. Cardiomyocyte NF-κB p65 promotes adverse remodelling, apoptosis, and endoplasmic reticulum stress in heart failure. *Cardiovasc Res*. 2011;89:129-138
3. Wang G, Hamid T, Keith RJ, Zhou G, Partridge CR, Xiang X, Kingery JR, Lewis RK, Li Q, Rokosh DG, Ford R, Spinale FG, Riggs DW, Srivastava S, Bhatnagar A, Bolli R, Prabhu SD. Cardioprotective and antiapoptotic effects of heme oxygenase-1 in the failing heart. *Circulation*. 2010;121:1912-1925
4. Lavelle GC, Sturman L, Hadlow WJ. Isolation from mouse spleen of cell populations with high specific infectivity for scrapie virus. *Infect Immun*. 1972;5:319-323
5. Austyn JM, Hankins DF, Larsen CP, Morris PJ, Rao AS, Roake JA. Isolation and characterization of dendritic cells from mouse heart and kidney. *J Immunol*. 1994;152:2401-2410
6. Fleming TJ, Fleming ML, Malek TR. Selective expression of Ly-6G on myeloid lineage cells in mouse bone marrow. RB6-8C5 mAb to granulocyte-differentiation antigen (Gr-1) detects members of the Ly-6 family. *J Immunol*. 1993;151:2399-2408

7. Robbins CS, Swirski FK. The multiple roles of monocyte subsets in steady state and inflammation. *Cell Mol Life Sci*. 2010;67:2685-2693
8. Gordon S, Taylor PR. Monocyte and macrophage heterogeneity. *Nat Rev Immunol*. 2005;5:953-964
9. Geissmann F, Manz MG, Jung S, Sieweke MH, Merad M, Ley K. Development of monocytes, macrophages, and dendritic cells. *Science*. 2010;327:656-661
10. Shortman K, Naik SH. Steady-state and inflammatory dendritic-cell development. *Nature reviews. Immunology*. 2007;7:19-30
11. Biswas SK, Mantovani A. Macrophage plasticity and interaction with lymphocyte subsets: Cancer as a paradigm. *Nat Immunol*. 2010;11:889-896
12. Kushwah R, Hu J. Complexity of dendritic cell subsets and their function in the host immune system. *Immunology*. 2011;133:409-419
13. Hadeiba H, Lahl K, Edalati A, Oderup C, Habtezion A, Pachynski R, Nguyen L, Ghodsi A, Adler S, Butcher EC. Plasmacytoid dendritic cells transport peripheral antigens to the thymus to promote central tolerance. *Immunity*. 2012;36:438-450
14. Hochrein H, O'Keeffe M, Wagner H. Human and mouse plasmacytoid dendritic cells. *Human Immunol*. 2002;63:1103-1110
15. Blasius AL, Colonna M. Sampling and signaling in plasmacytoid dendritic cells: The potential roles of Siglec-H. *Trends Immunol*. 2006;27:255-260
16. Ito T, Yang M, Wang YH, Lande R, Gregorio J, Perng OA, Qin XF, Liu YJ, Gilliet M. Plasmacytoid dendritic cells prime IL-10-producing T-regulatory cells by inducible costimulator ligand. *J Exp Med*. 2007;204:105-115
17. Kitchen SG, Jones NR, LaForge S, Whitmire JK, Vu BA, Galic Z, Brooks DG, Brown SJ, Kitchen CM, Zack JA. CD4 on CD8+ T cells directly enhances effector function and is a target for HIV infection. *Proc Natl Acad Sci USA*. 2004;101:8727-8732
18. Ismahil MA, Hamid T, Haberzettl P, Gu Y, Chandrasekar B, Srivastava S, Bhatnagar A, Prabhu SD. Chronic oral exposure to the aldehyde pollutant acrolein induces dilated cardiomyopathy. *Am J Physiol Heart Circ Physiol*. 2011;301:H2050-2060
19. Wang HX, Yi SQ, Li J, Terayama H, Naito M, Hirai S, Qu N, Yi N, Itoh M. Effects of splenectomy on spontaneously chronic pancreatitis in aly/aly mice. *Clin Dev Immunol*. 2010;2010:614890
20. Kodama M, Matsumoto Y, Fujiwara M. In vivo lymphocyte-mediated myocardial injuries demonstrated by adoptive transfer of experimental autoimmune myocarditis. *Circulation*. 1992;85:1918-1926

Supplemental Table I. Forward and Reverse Primers for Real-Time PCR

Gene Name	*Gene ID*	*Accession #*	*Sequence*
TNF-α	21296	NM_013693	F: CAGCCGATGGGTTGTACCTT R: GGCAGCCTTGTCCCTTGA
IL-1β	16176	NM_008361	F: AGTTGACGGACCCCAAAAGA R: GGACAGCCCAGGTCAAAGG
IL-2	16183	NM_008366	F: AAACTAAAGGGCTCTGACAACACA R: CACCACAGTTGCTGACTCATCA
IL-4	16189	NM_021283	F: GGAGATGGATGTGCCAAACG R: CGAGCTCACTCTCTGTGGTGTT
IL-5	16191	NM_010558	F: TGCACTTGAGTGTTCTGACTCTCA R: TGTGCTCATGGGAATCTCCAT
IL-6	16193	NM_031168	F: CCACGGCCTTCCCTACTTC R: TTGGGAGTGGTATCCTCTGTGA
IL-10	16153	NM_010548	F: GATGCCCCAGGCAGAGAA R: CACCCAGGGAATTCAAATGC
IL-13	16163	NM_008355	F: TTGAGGAGCTGAGCAACATCAC R: CCATGCTGCCGTTGCA
IFN-γ	15978	NM_008337	F: TTGGCTTTGCAGCTCTTCCT R: TGACTGTGCCGTGGCAGTA
iNOS	18126	NM_010927	F: AGACCTCAACAGAGCCCTCA R: GCAGCCTCTTGTCTTTGACC
CCR2	12772	NM_009915	F: CTGCTCAACTTGGCCATCTCT R: GTGAGCCCAGAATGGTAATGTG
CCR5	12774	NM_009917	F: GTCAAACGCTTTTGCAAACG R: TGAGCTTGCACGATCAGGATT
CCL5	20304	NM_013653	F: TCCAATCTTGCAGTCGTGTTTG R: TCTGGGTTGGCACACACTTG
CXCR3	12766	NM_009910	F: TTGCCCTCCCAGATTTCATC R: TGGCATTGAGGCGCTGAT
CX3CR1	13051	NM_009987	F: TCGGTCTGGTGGGAAATCTG R: GGCTTCCGGCTGTTGGT
TLR1	21897	NM_001276445	F: GGCTTTGCAGGAACTCAATGTA R: CCCCGCACCCAGGAA
TLR7	170743	NM_133211	F: CAGTGAACTCTGGCCGTTGA R: CAAGCCGGTTGTTGGAGAA
TLR9	81897	NM_031178	F: CCTTCGTGGTGTTCGATAAGG R: CACCCGCAGCTCGTTATACA
TLR12	384059	NM_205823	F: CTGCCACTGTGCCAATGC

			R: ATATGTACGTTTTAGTGGACCGCTTA
TGF-β	21803	NM_011577	F: GCAGTGGCTGAACCAAGGA R: AGCAGTGAGCGCTGAATCG
HMGB1	15289	NM_010439	F: CCCCAATGCACCCAAGAG R: GGCGGTACTCAGAACAGAACAAG
Galectin-3	16854	NM_001145953	F: CACAATCATGGGCACAGTGAA R: TTCCCTCTCCTGAAATCTAGAACAA
S100A8	20201	NM_013650	F: GGCCTTGAGCAACCTCATTG R: AGAGGGCATGGTGATTTCCTT
S100A9	20202	NM_009114	F: TCATGGAGGACCTGGACACA R: CAGCATCATACACTCCTCAAAGCT

SUPPLEMENTAL FIGURE LEGENDS

Supplemental Figure I. Long-term pathological cardiac remodeling after coronary ligation. ***A,*** Representative M-mode echocardiograms (*Left*) and Masson's trichrome-stained short-axis histological sections (*Right*) from sham-operated mice and mice with permanent coronary ligation and heart failure (HF), 8 weeks after operation. Histological images were taken with a 2X objective; scale bar 1 mm. ***B*****,** Higher power histological images of trichrome (left) and Alexa Fluor 488-conjugated wheat-germ agglutinin (WGA) stains of sham and HF heart sections. ***C***, quantitative group data for gravimetric, histological, and echocardiographic analyses from sham and HF mice. EDV and ESV, end-diastolic and end-systolic volume; EF, ejection fraction. Fibrosis and myocyte area were determined in myocardium remote from the infarction. N = 5-7/group.

Supplemental Figure II. Serum cytokine levels in sham and HF mice as determined by cytometric bead array immunoassay. IL, interleukin; TNF, tumor necrosis factor; IFN, interferon, MCP, monocyte chemotactic protein. N = 3-4/group.

Supplemental Figure III. Representative flow cytometry scatter plots for SSC versus Siglec-H fluorescence in mononuclear splenocytes from sham and HF mice, expressed as percentage of the total mononuclear cell population, and corresponding group data. An unstained control sample (*Left*) is also shown for comparison. N = 4-5/group.

Supplemental Figure IV. Representative live cell gates and scatter plots from sham and HF spleens identifying $CD3^+CD4^+$ and $CD3^+CD8^+CD4^-$ cells as a percentage of total live mononuclear cell population, and corresponding group data. N = 4-5/group.

Supplemental Figure V. Quantitative group data for activated monocytes ($Lin2^-CD11b^+F4/80^+$ cells), classical DCs ($Lin1^-CD11c^+B220^-$ cells), and plasmacytoid DCs ($Lin1^-CD11c^{+/low}B220^+$ cells) in bone marrow from sham and HF mice. N = 5-6/group.

Supplemental Figure VI. Serum cytokine levels as determined by cytometric bead array immunoassay in mice with HF (16 weeks after coronary ligation) that underwent either

splenectomy (HF without spleen) or sham abdominal surgery (HF with spleen) 8 weeks after ligation. All values normalized to HF with spleen group. TNF, tumor necrosis factor; MCP, monocyte chemotactic protein; IL, interleukin; IFN, interferon. N = 4-6/group.

Supplemental Figure VII. Representative peripheral blood leukocyte flow cytometry scatter plots for recipient $CD45.1^+$ versus donor $CD45.2^+$ cells (monocyte-lymphocyte gate) two weeks following splenocyte adoptive transfer (AT) demonstrating low levels of residual circulating $CD45.2^+$ donor cells (1.56% in this example). An unstained blood sample is shown for comparison.

Supplemental Figure VIII. Serum cytokine levels as determined by cytometric bead array immunoassay in mice that received either sham-splenocytes or HF-splenocytes, measured 8 weeks after adoptive transfer. All values normalized to sham-splenocyte group. TNF, tumor necrosis factor; MCP, monocyte chemotactic protein; IL, interleukin; IFN, interferon. N = 3-5/group.

Supplemental Figure IX. ***A,*** $Lin2^-CD11b^+F4/80^+$ circulating monocytes were identified from the monocyte-lymphocyte gate of peripheral blood leukocytes from mice treated with either lipopolysaccharide (LPS) or PBS control for two days. $CD11b^+F4/80^+$ cells were then subdivided as Gr-1 low or high. Representative scatter plots from PBS and LPS treated mice (and unstained sample control) are shown in the top panels and quantitative group data for circulating monocyte subsets in the bottom panels. N = 5/group. ***B***, Representative M-mode echocardiograms from recipient mice given mononuclear splenocytes from either PBS- or LPS-treated mice, at baseline (prior to transfer) and 8 weeks after adoptive cell transfer.

Supplemental Figure X. Normalized gene expression of select pro- and anti-inflammatory mediators and TLR pattern-recognition receptors (PRRs) in mononuclear splenocytes isolated from sham-operated and HF mice. *$p < 0.05$ vs. sham; n = 4-6/group.

Supplemental Figure XI. ***A***, Representative splenic immunostains for the alarmin HMGB1 from sham-operated and HF mice and corresponding quantitation for HMGB1

fluorescence intensity. WP, white pulp, RP, red pulp, MZ, marginal zone. ***B***, Normalized gene expression of the alarmins HMGB1, S100A8, S100A9, and galectin-3 in mononuclear splenocytes isolated from sham and HF mice. n = 4-5/group for ***A*** and ***B***. ***C,*** Representative confocal images of HMGB1 (green), CD45.2 (red), and DAPI (blue, for nuclei) (immuno)staining of hearts from CD45.1 mice 8 weeks after adoptive transfer of CD45.2 sham- or HF-splenocytes. The yellow arrow indicates a $CD45.2^{+}HMGB1^{+}$ cell cluster in the HF-splenocyte recipient heart. The green arrows indicate other areas of HMGB1 expression in recipient myocardium.

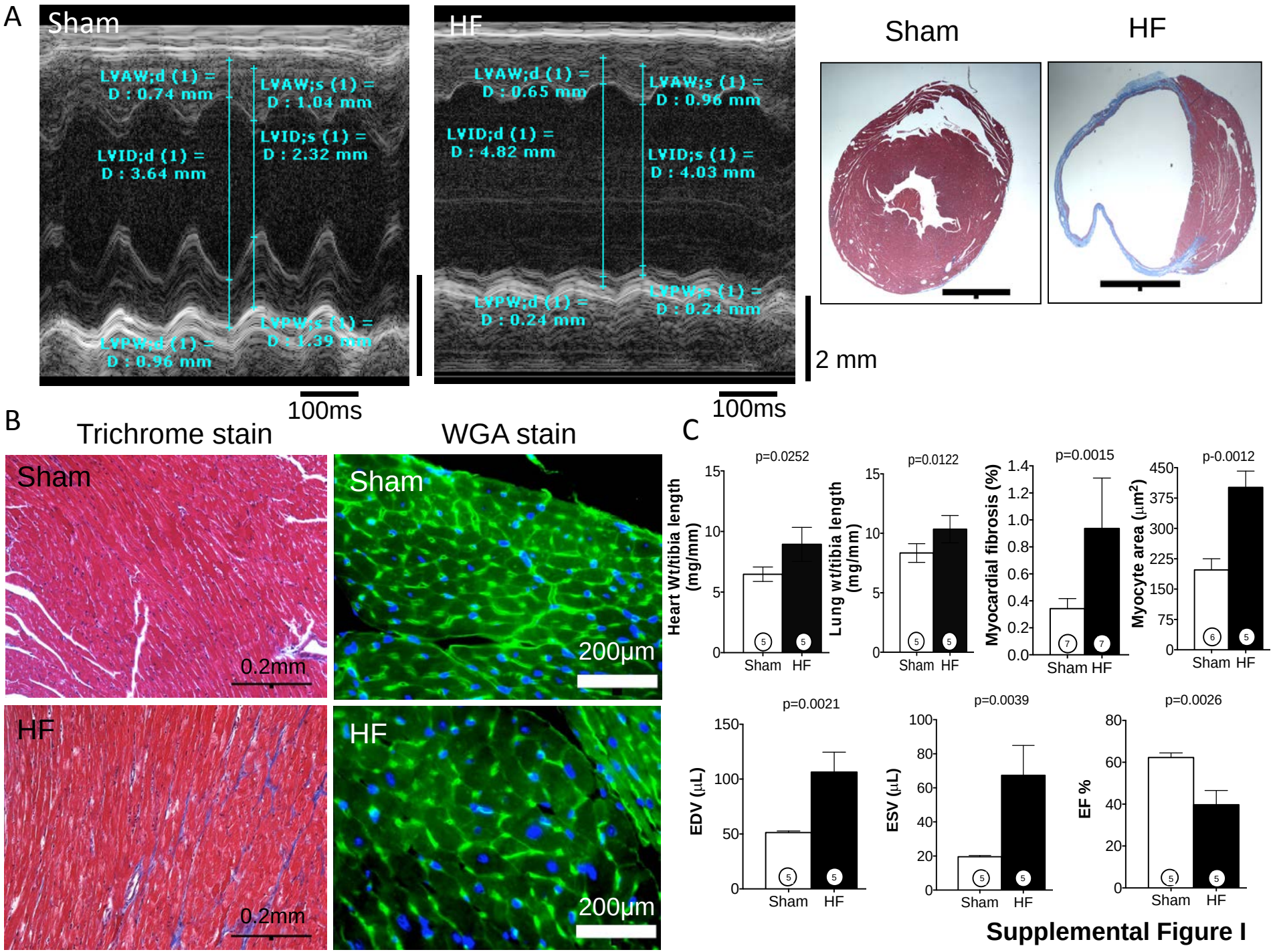

Supplemental Figure I

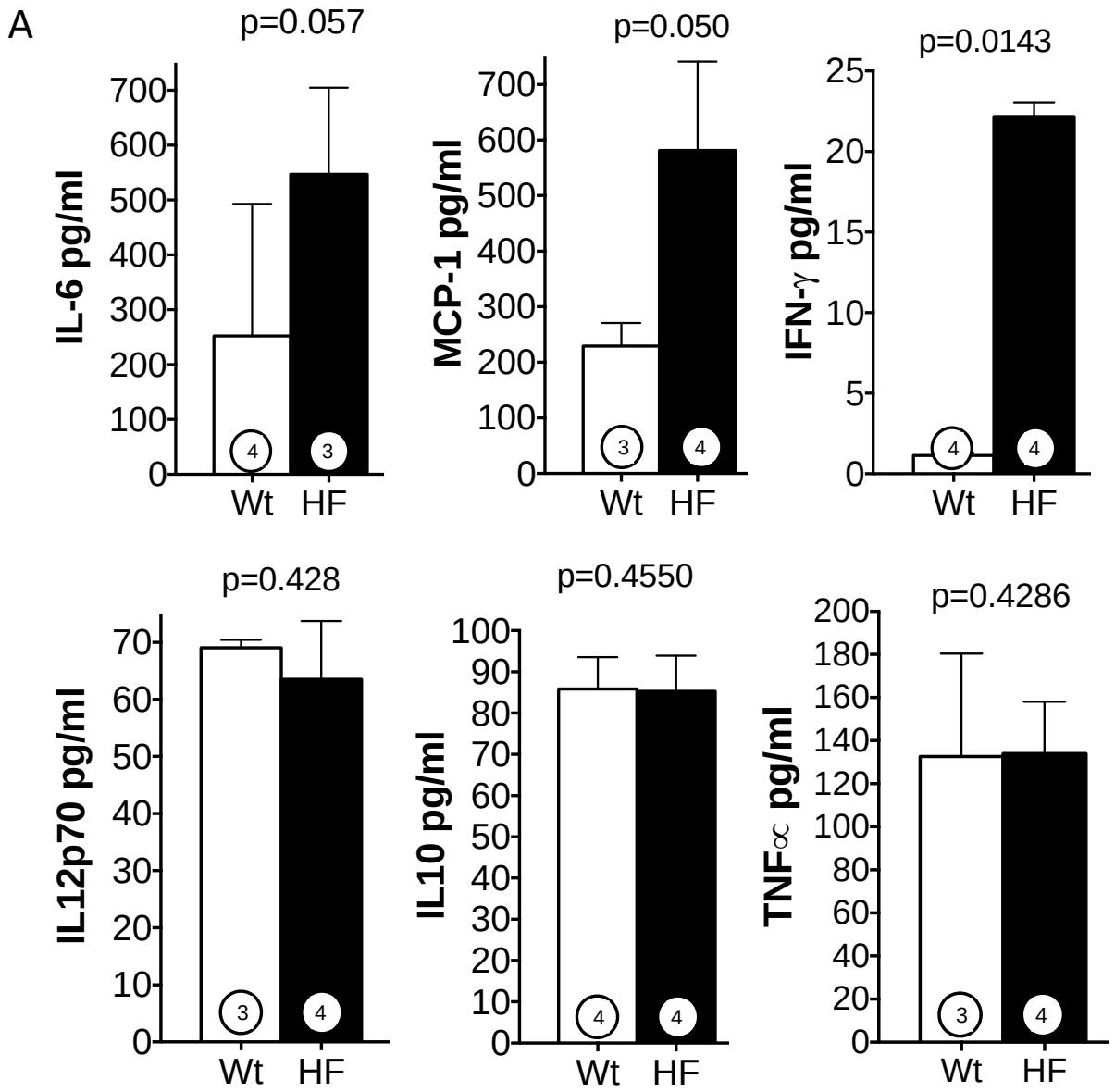

Supplemental Figure II

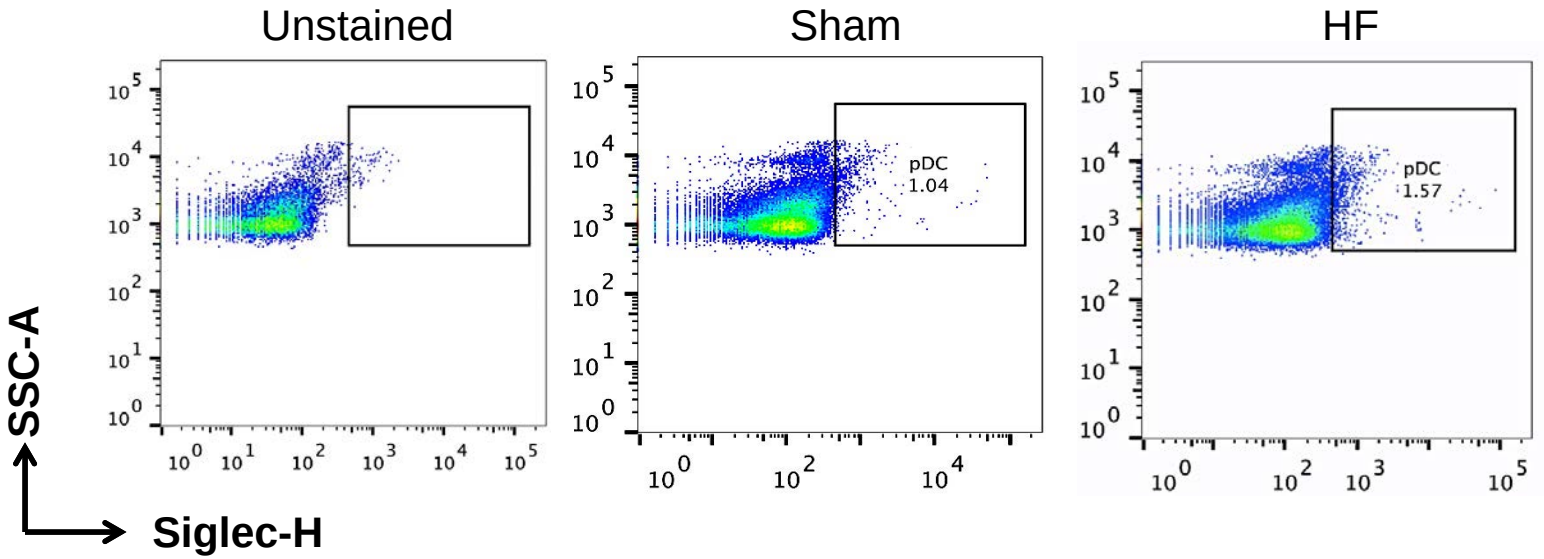

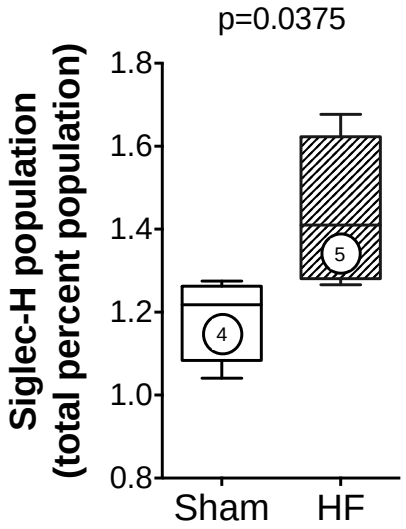

Supplemental Figure III

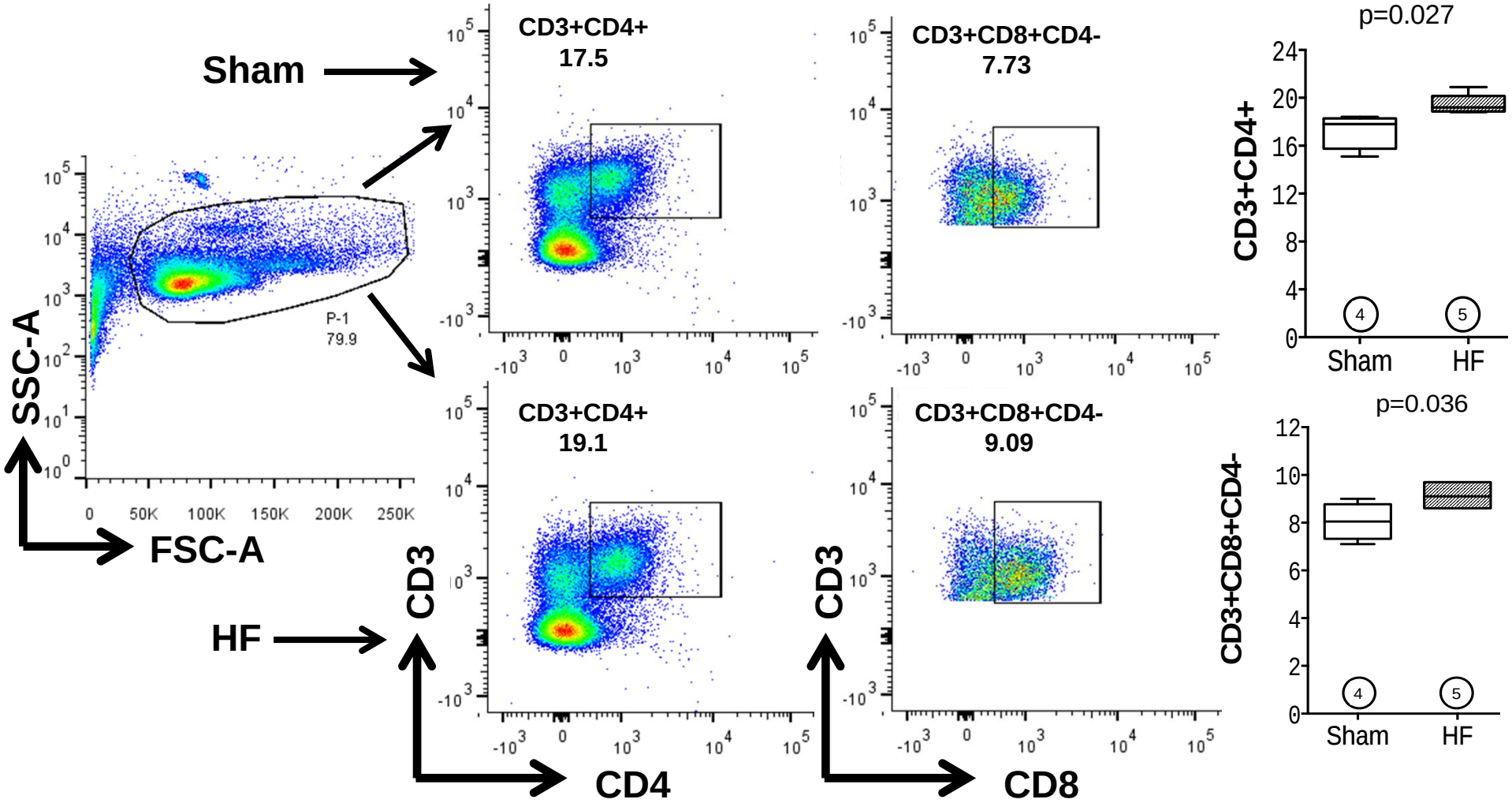

Supplemental Figure IV

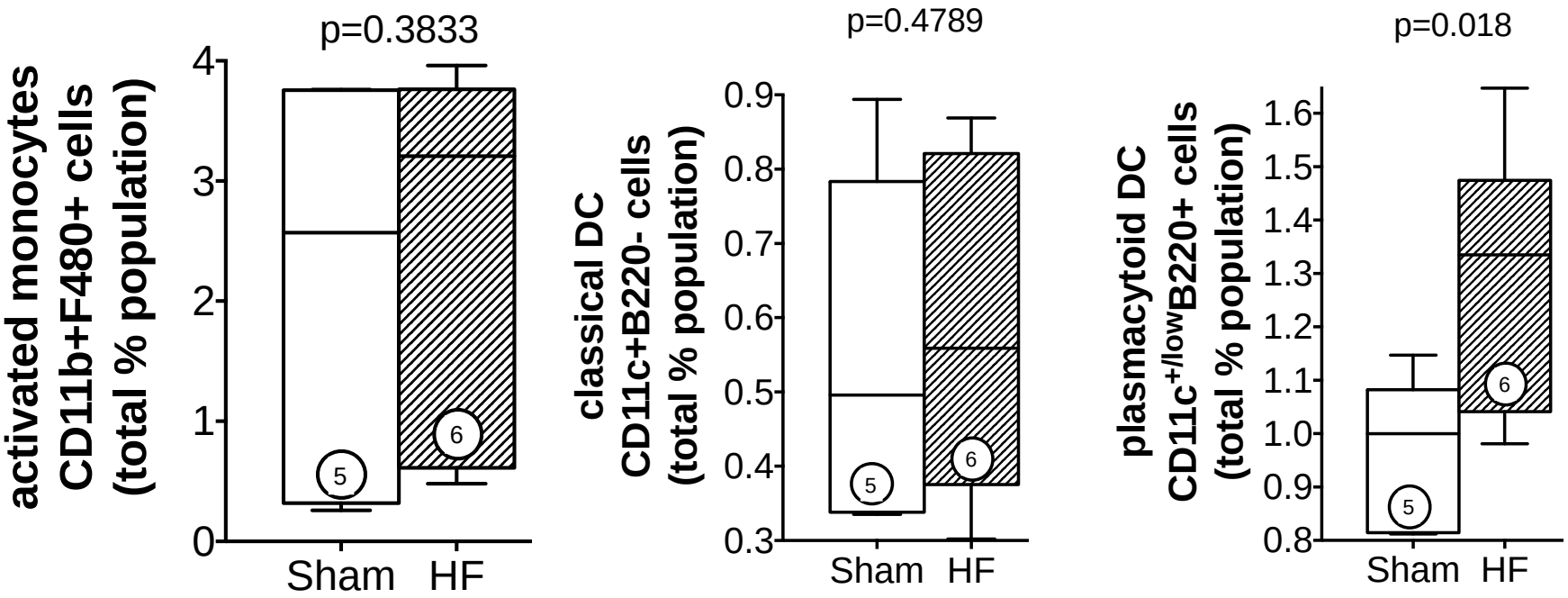

Supplemental Figure V

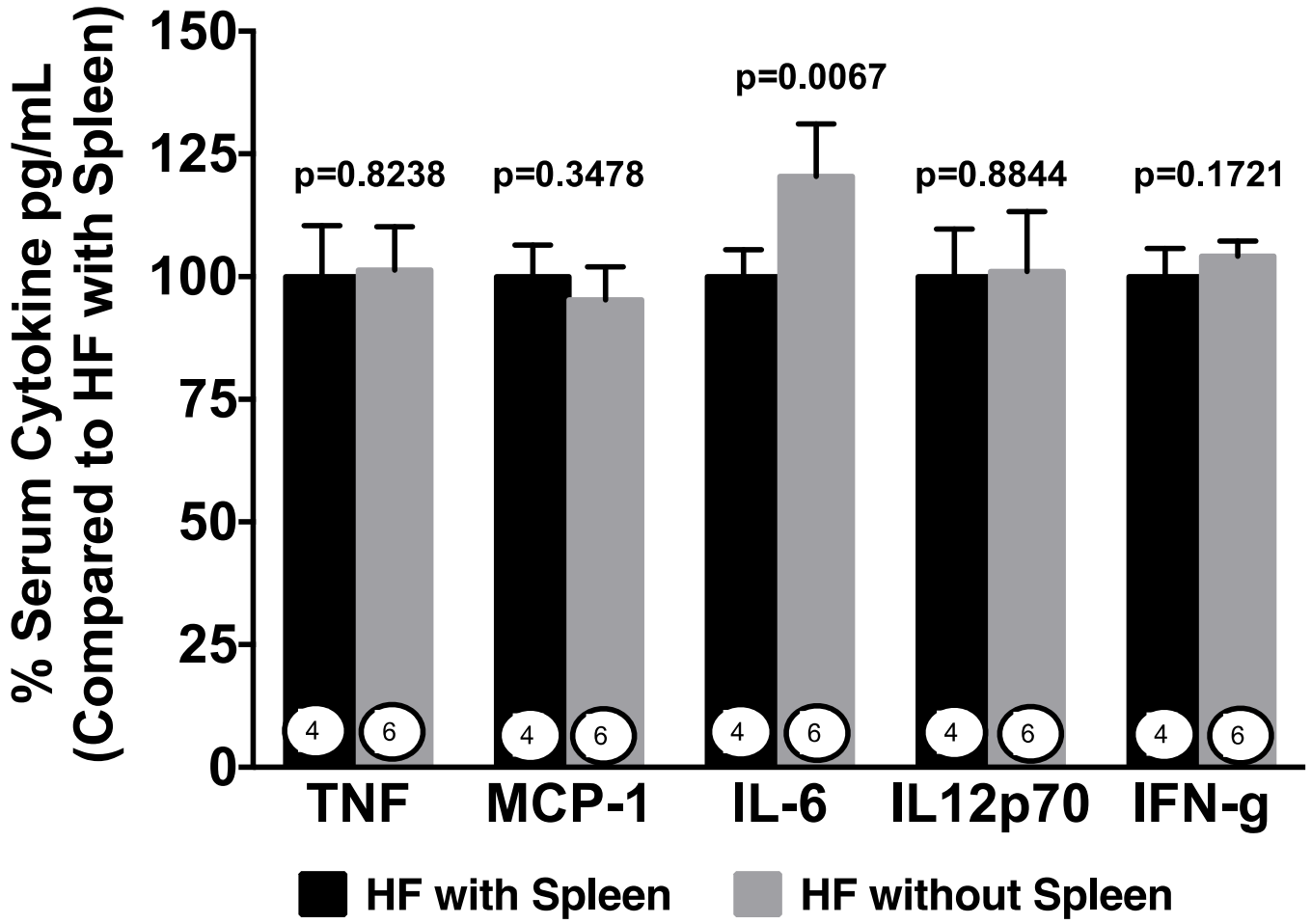

Supplemental Figure VI

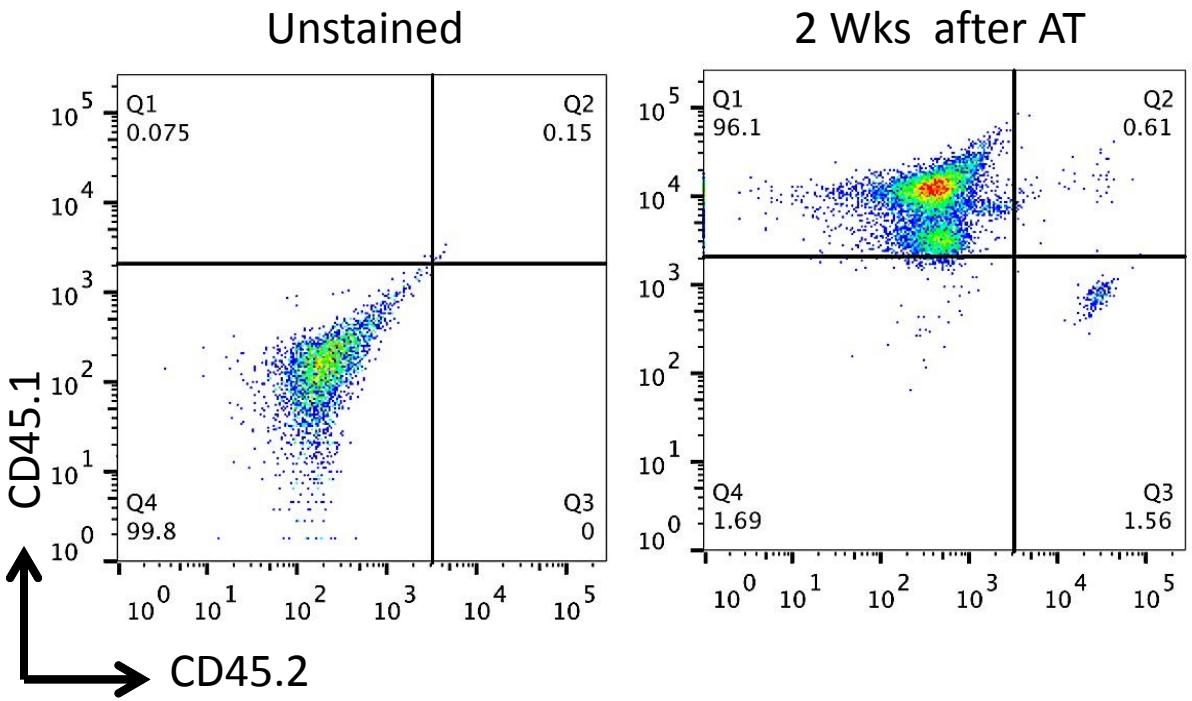

Supplemental Figure VII

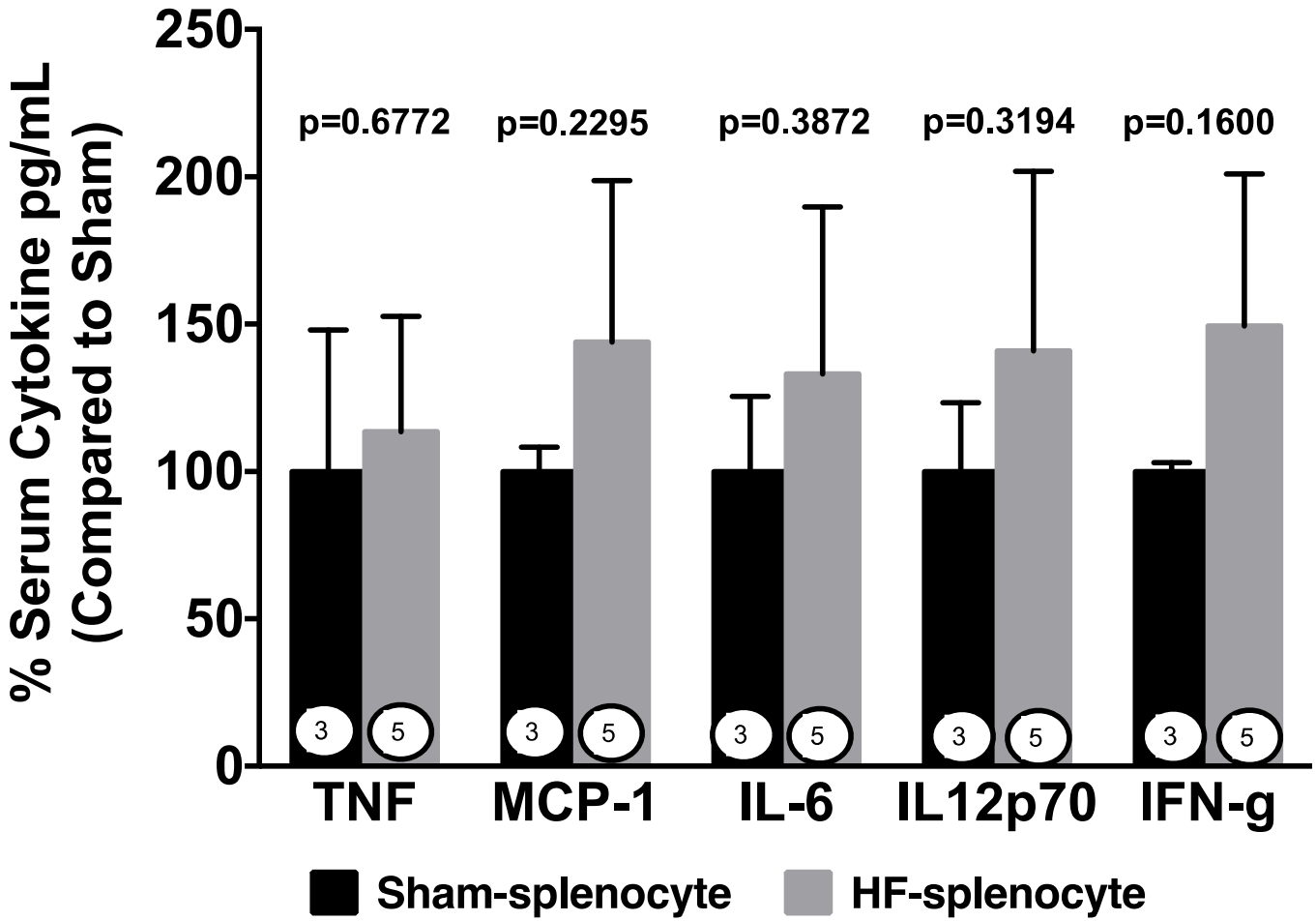

Supplemental Figure VIII

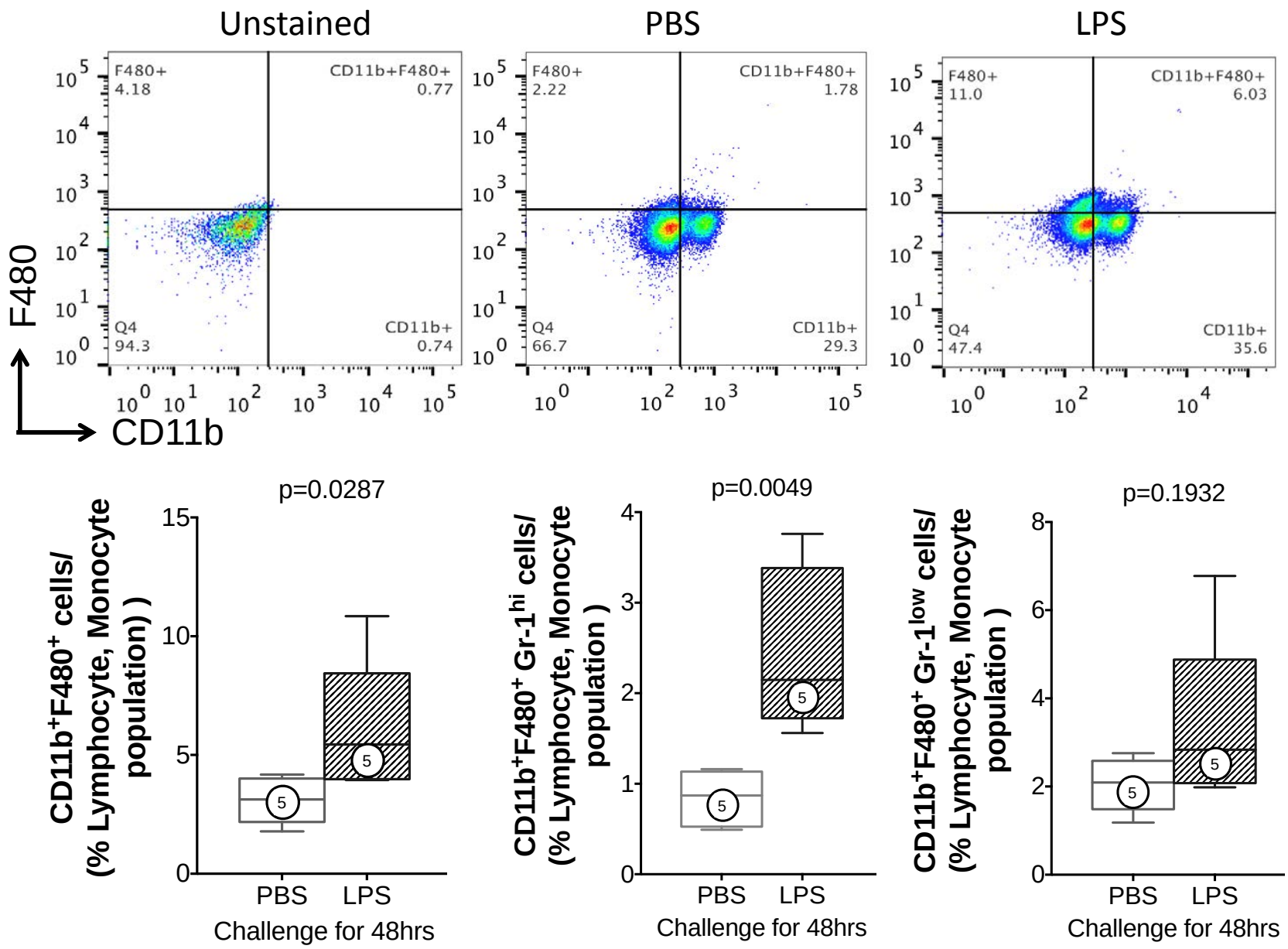

Supplemental Figure IX*A*

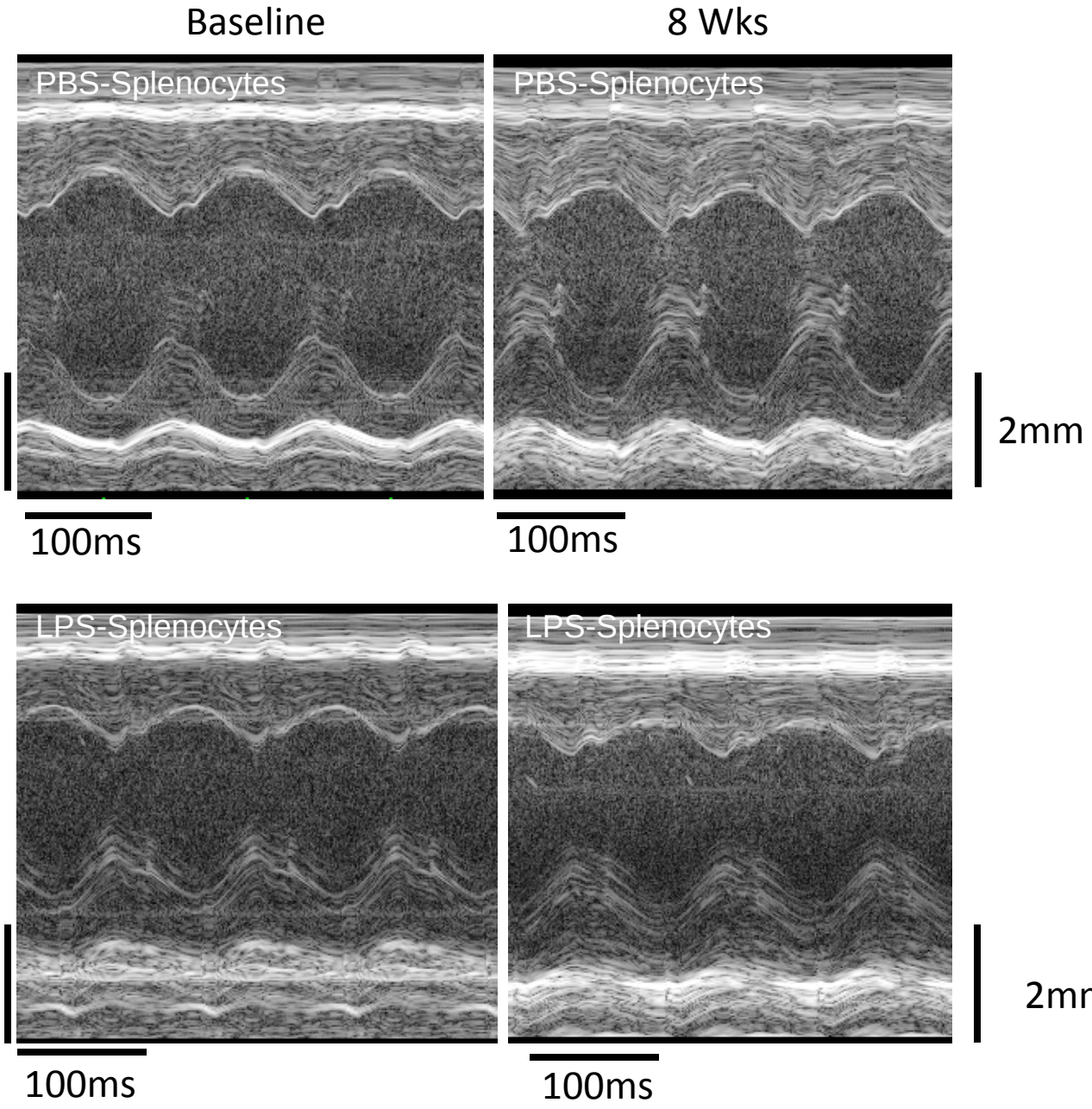

Supplemental Figure IX*B*

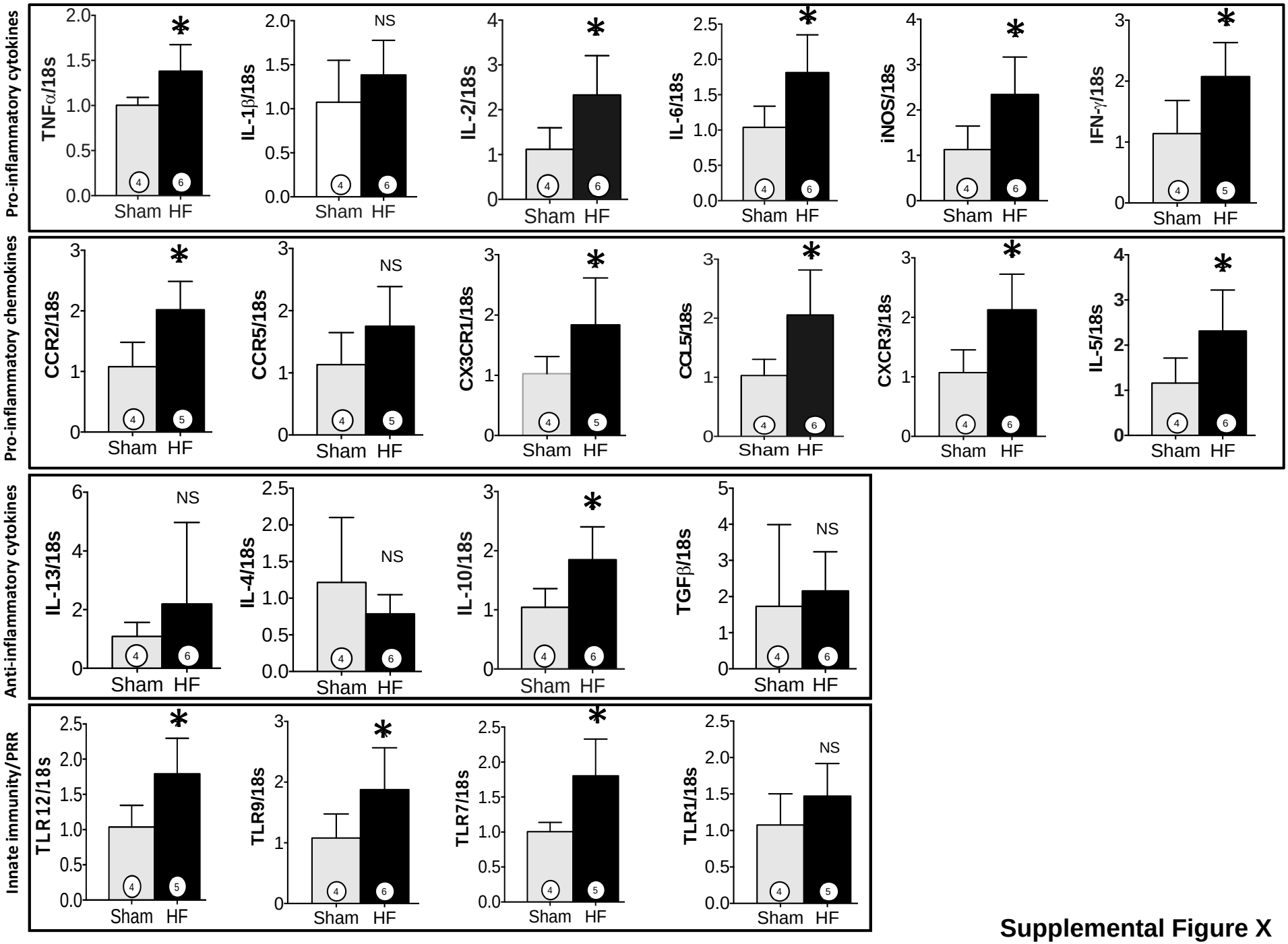

Supplemental Figure X

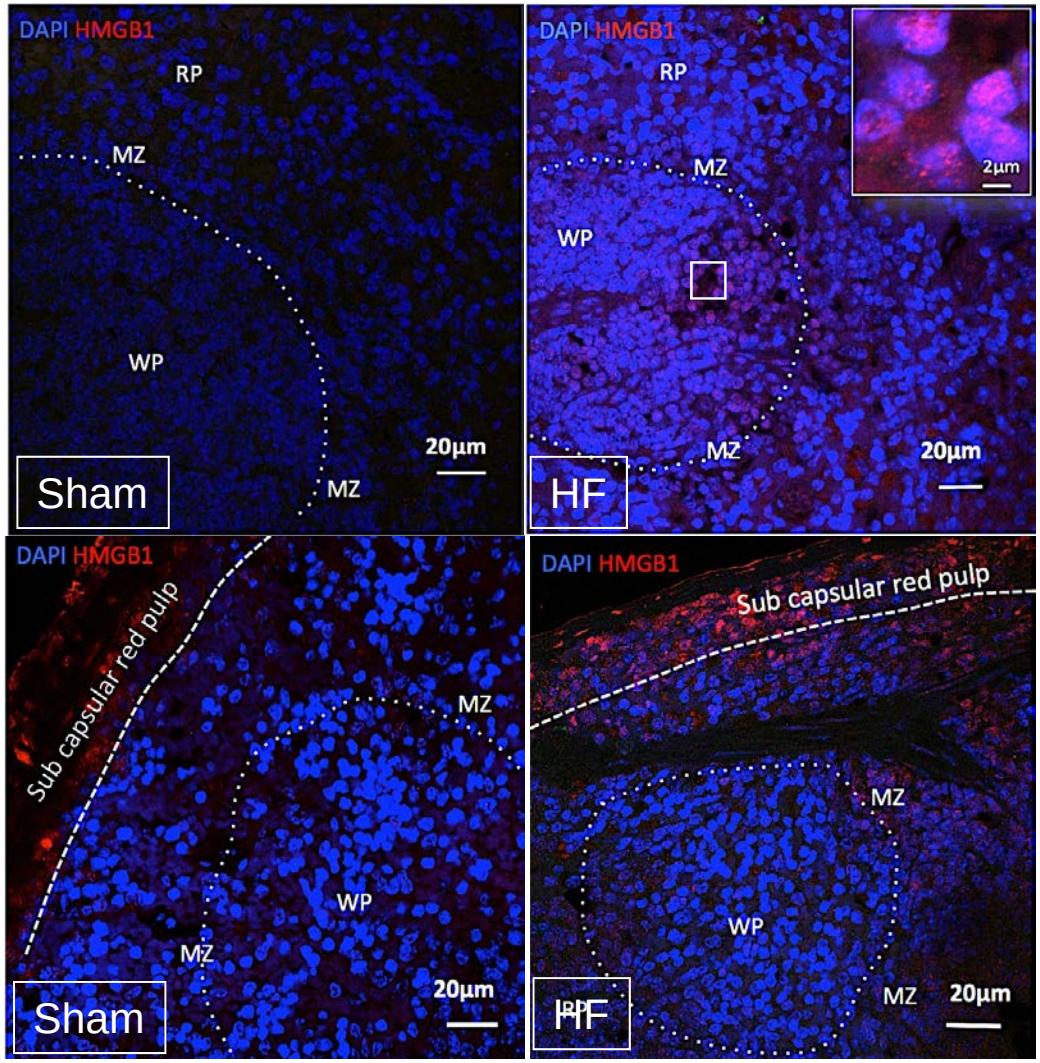

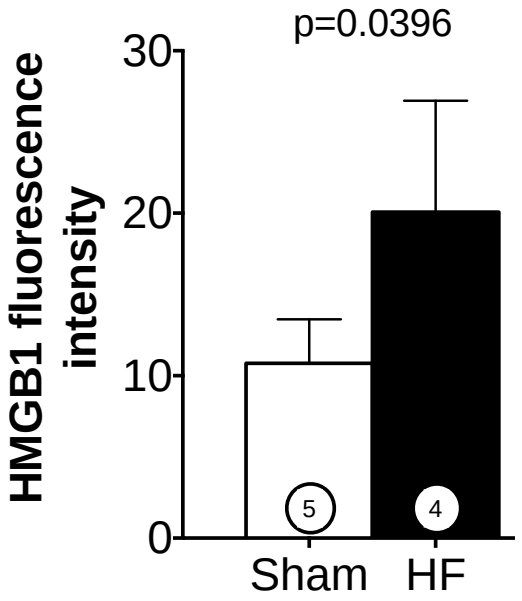

Supplemental Figure XI*A*

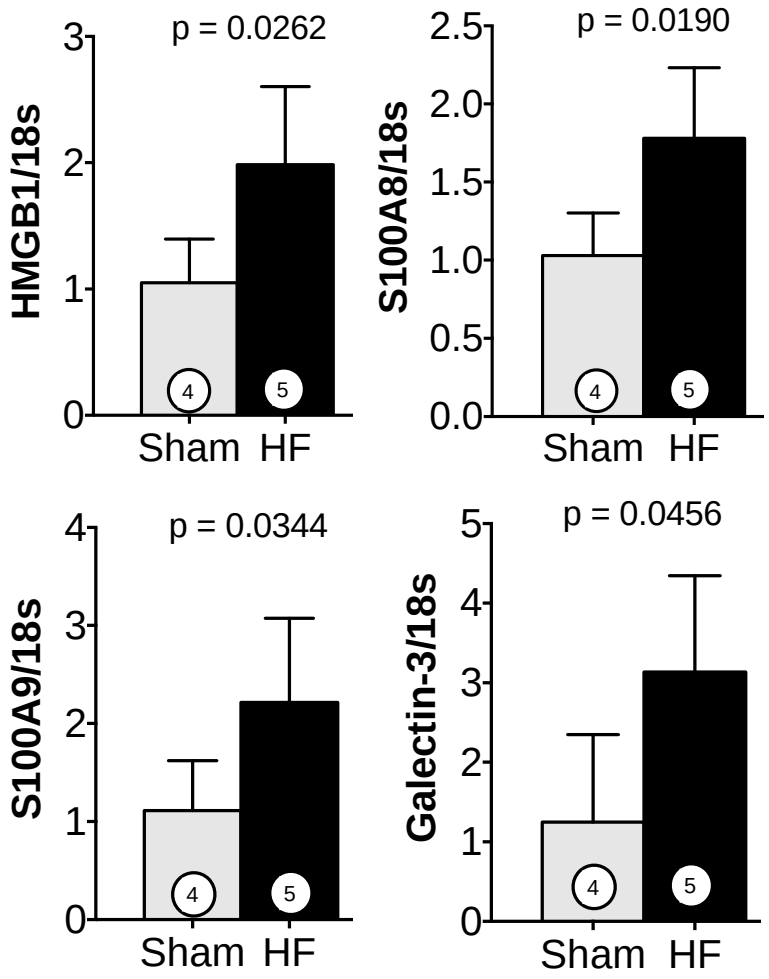

Supplemental Figure XI*B*

F

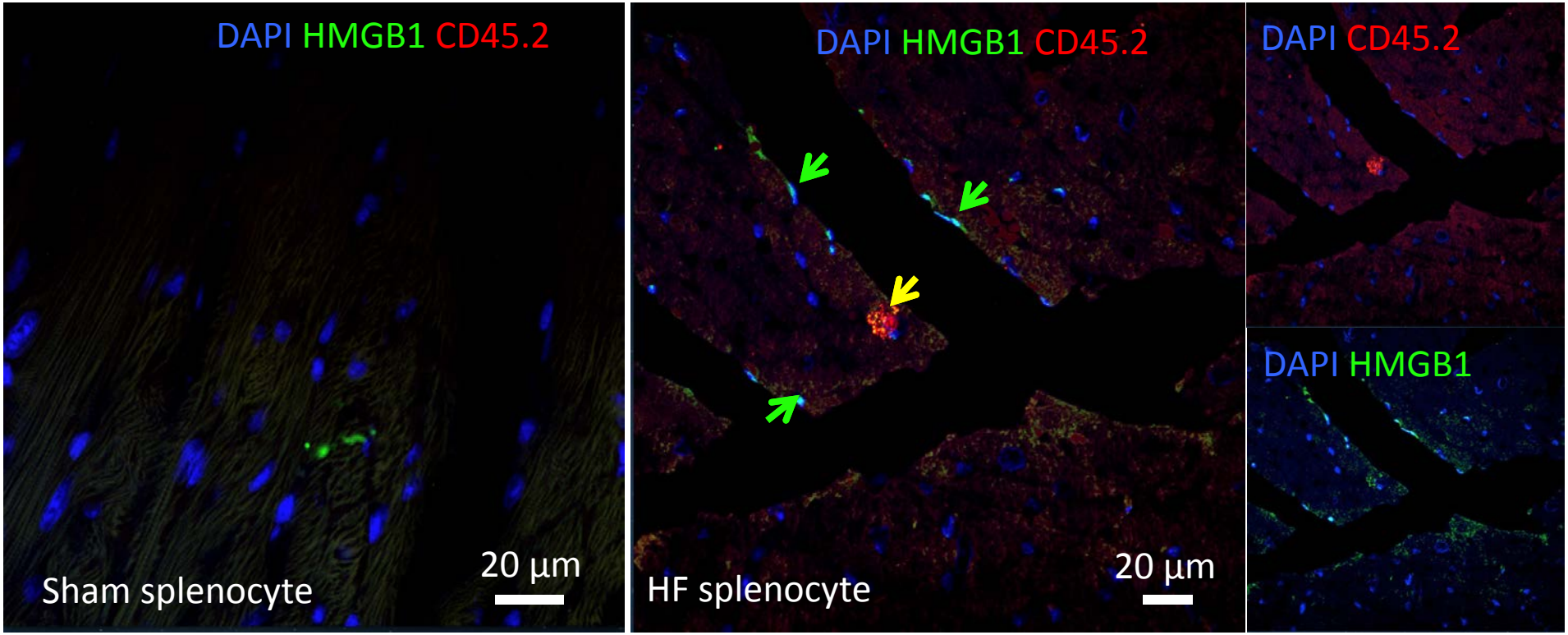

Supplemental Figure XIC